



Variability in martian sinuous ridge form: Case study of Aeolis Serpens in the Aeolis Dorsa, Mars, and insight from the Mirackina paleoriver, South Australia

Rebecca M.E. Williams^{a,*}, Rossman P. Irwin III^b, Devon M. Burr^c, Tanya Harrison^{d,1}, Phillip McClelland^e

^a Planetary Science Institute, Tucson, AZ 85719-2395, United States

^b Center for Earth and Planetary Studies, Smithsonian Institution, Washington, DC 20013-7012, United States

^c Earth and Planetary Sciences, University of Tennessee, Knoxville, TN 37996-1410, United States

^d Malin Space Science Systems, San Diego, CA 92121, United States

^e Ultramag Geophysics, Mount Hutton, NSW 2280, Australia

ARTICLE INFO

Article history:

Received 3 August 2012

Revised 6 March 2013

Accepted 10 March 2013

Available online 2 April 2013

Keywords:

Mars, Surface

Geological processes

Earth

ABSTRACT

In the largest known population of sinuous ridges on Mars, Aeolis Serpens stands out as the longest (~500 km) feature in Aeolis Dorsa. The formation of this landform, whether from fluvial or glacio-fluvial processes, has been debated in the literature. Here we examine higher-resolution data and use a terrestrial analog (the Mirackina paleoriver, South Australia) to show that both the morphology and contextual evidence for Aeolis Serpens are consistent with development of an inverted fluvial landform from differential erosion of variably cemented deposits. The results of this study demonstrate that the induration mechanism can affect preservation of key characteristics of the paleoriver morphology. For groundwater cemented inverted fluvial landforms, like the Mirackina example, isolated remnants of the paleoriver are preserved because of the temporal and spatial variability of cementation sites. Upon landscape inversion, the result is a landform comprised of aligned mesas and ridges with an undulating longitudinal profile. Recognizing how different induration mechanisms affect preservation of fluvial sediments in denuded regions is relevant to the interpretation of sinuous ridges at other locations on Mars. In particular, double ridge transverse shape may be an instrumental aspect in identifying potential inverted fluvial landforms. There are significant limitations on determining former channel parameters for inverted fluvial landforms that form as a result of variable cementation. Radius of curvature can be accurately determined and an upper-bound constraint for former channel wavelength and width can be made, but it is not possible to reconstruct the paleoslope. Thus, the number of applicable paleohydrologic models is restricted and only first order estimates of flow magnitude can be made. Paleodischarge estimates range between 10^2 and 10^3 m³/s for both Aeolis Serpens and the Mirackina paleoriver. Located near the base of the Medusae Fossae Formation (MFF), Aeolis Serpens provides insight into the fluvial environment early in the development of that deposit. When Aeolis Serpens was active, climate conditions must have included at least a period conducive to channelized flow for several hundred kilometers.

© 2013 Elsevier Inc. All rights reserved.

1. Introduction

'Sinuous ridge' is a non-genetic term applied to elongate, positive-relief landforms on Mars that have a curved planform (e.g., Kargel and Strom, 1991). Sinuous ridges have been identified at a number of sites on Mars (e.g., Williams, 2007), including on large-scale alluvial fans (Moore and Howard, 2005), on several plateaus surrounding the Valles Marineris canyon system (LeDeit et al., 2010; Weitz et al., 2010), in Sinus Meridiani and Arabia Terra

(e.g., Edgett, 2005; Williams and Chuang, 2012), in the Argyre basin, (Kargel and Strom, 1992), near the south pole (e.g., Kargel, 1993; Head, 2000a, 2000b; Head and Pratt, 2001; Ghatan and Head, 2004), as part of a fan-shaped complex within Eberswalde crater (Malin and Edgett, 2003; Moore et al., 2003), on an alluvial fan near the Mars Science Laboratory landing site in Gale crater (Anderson and Bell, 2010), and in Aeolis Dorsa (Burr et al., 2009).

Multiple hypotheses for martian sinuous ridges have been proposed, including wrinkle ridges and lava flows (Tanaka and Scott, 1987), exhumed igneous dikes (Carr and Evans, 1980), exhumed clastic dikes (Ruff and Greeley, 1990), eskers (e.g., Howard, 1981; Kargel and Strom, 1992; Kargel, 2004, pp. 139–159; Banks et al., 2009), glacial moraines (e.g., Hiesinger and Head, 2002; Lang, 2007), and inverted stream channels (e.g., Howard, 1981; Williams and Edgett, 2005; Pain et al., 2007; Burr et al., 2009). The morpho-

* Corresponding author. Address: 1700 East Fort Lowell, Suite 106, Planetary Science Institute, Tucson, AZ 85719, United States. Fax: +1 520 622 8060.

E-mail address: williams@psi.edu (R.M.E. Williams).

¹ Present address: Department of Earth Sciences/Centre for Planetary Science and Exploration, Western University, London, ON, N6A 5B7.

logical characteristics and geologic context for each sinuous ridge must be assessed to accurately interpret the formation history of the landform and infer associated climatic conditions.

One of the highest concentrations of sinuous ridges on Mars, Aeolis Dorsa, is found along the crustal dichotomy boundary within the Aeolis and Zephyria Plana region between the two westernmost lobes of the Medusae Fossae Formation (MFF; Fig. 1). The MFF is dated to the Amazonian Period by several studies (e.g., Scott and Tanaka, 1986; Tanaka, 1986; Zimbelman, 2011), although recent work indicates that a significant part of the MFF may have been emplaced during the Hesperian Period (Kerber and Head, 2010; Zimbelman and Scheidt, 2012). Either way, the stratigraphic position of the sinuous ridges in Aeolis Dorsa places them among the youngest such landforms on Mars (see also Section 4.4; Burr et al., 2009).

The first categorization of sinuous ridge morphology in Aeolis Dorsa was conducted by Burr et al. (2009) based largely on visible-band images from the Thermal Emission Imaging System (THEMIS-VIS; 18 meter per pixel; Christensen et al., 2004) instrument, with some higher-resolution characterization based on scattered Mars Orbiter Camera (MOC; Malin et al., 2010) and ConTeXt (CTX; Malin et al., 2007) images. Burr et al. (2009) classified

~150 sinuous ridges in the Aeolis/Zephyria Plana region into five main morphological crest types (flat-topped, thin, wispy, multi-level and rounded). An on-going survey based on ~80% coverage of the region by CTX data shows a factor of about six times the previous number of sinuous ridges, bringing the total to 890 sinuous ridge segments (Jacobsen and Burr, 2012). A small part of this increase is due to the revised approach of classifying a multi-level sinuous ridge (composed of both a lower and an upper sinuous ridge) as two separate features (Jacobsen and Burr, 2012). Collectively, Burr et al. (2009) interpreted the majority of sinuous ridges here as inverted fluvial channels.

However, an alternative explanation was proposed for the rounded sinuous ridge sub-class. This class represented 5% of sinuous ridges within the study region in seven disconnected THEMIS VIS images, although the THEMIS day IR mosaic was used in that work to suggest that these features were part of a single, continuous landform (Burr et al., 2009). (One additional rounded sinuous ridge is part of a separate fan landform). This long sinuous ridge was recently named Aeolis Serpens by the International Astronomical Union. (The IAU adopted the term 'serpens' for sinuous features with segments of positive and negative relief along their lengths.) Based on the isolated network pattern, apparent rounded shape, and local maxima in ridge elevation, Aeolis Serpens (Figs. 1 and 2) was tentatively hypothesized to be an esker (Burr et al., 2009; Zimbelman and Griffin, 2010). Subsequent analysis identified potential tributaries to Aeolis Serpens and reaches with paired lateral ridges, discounted an esker origin, and offered some inverted fluvial paleochannels in the Atacama Desert as visual analogs (Lefort et al., 2012).

In the present study presented below, we reassess this atypically long sinuous ridge using new higher resolution image and topographic data combined with insight derived from field investigation of an analog on Earth. The objective of this study is to evaluate proposed formation mechanisms for Aeolis Serpens through detailed study of the entire landform. We document variability in landform shape using image and topographic data. In addition,

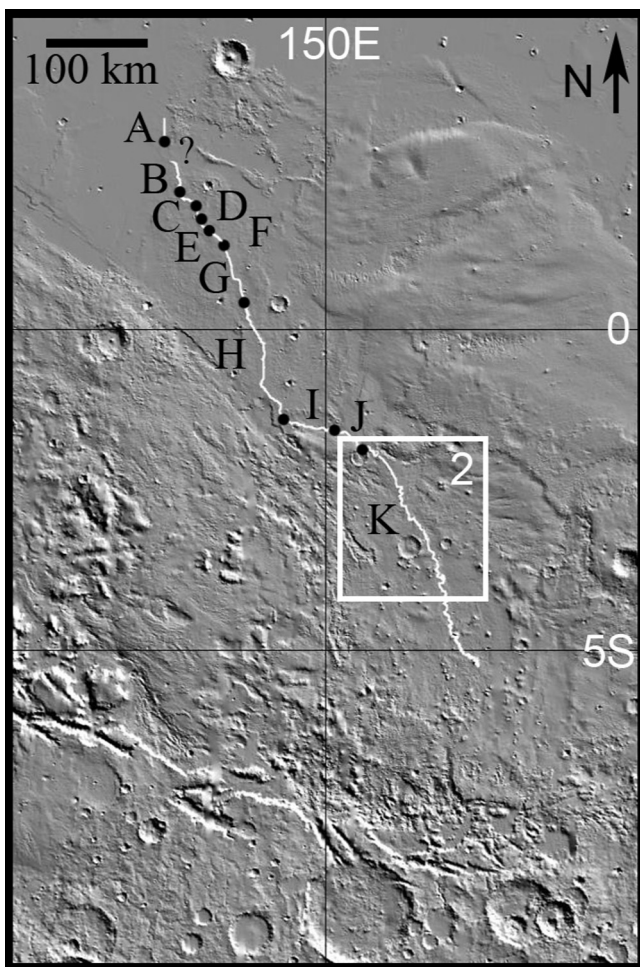


Fig. 1. Aeolis Serpens is marked in white on the shaded relief map of the Aeolis/Zephyria Planum region, Mars. Note that Lefort et al. (2012) extend the path of Aeolis Serpens farther south; the representation here ends at approximately 5.20°S, 152.33°E where there is possible burial of the landform. Black dots separate each morphology section (labeled by letters, see Table 1) determined in CTX image assessment. Ambiguous region in the northern part is marked by '?' as the path of the sinuous ridge landform is unclear. White box marks location of Fig. 2. Bounds are 5°N to 10°S, 145° to 155°E and the grid spacing is 5°. North is up in all figures.

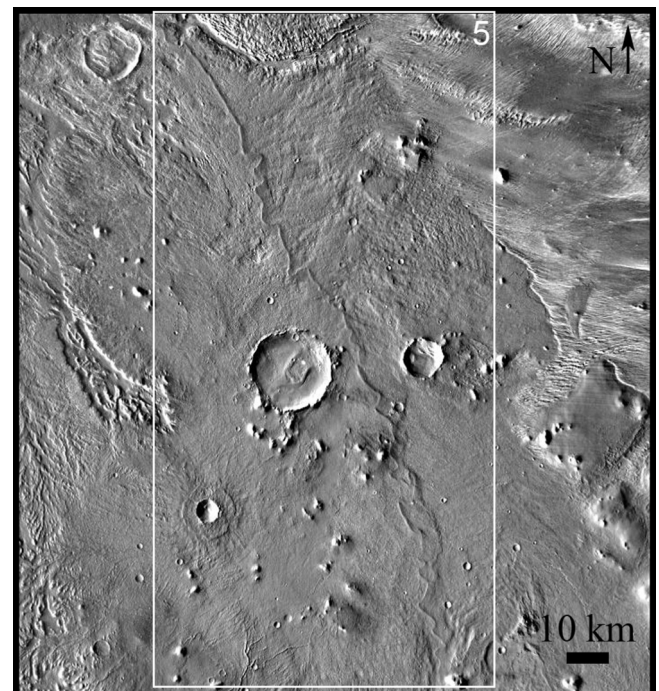


Fig. 2. The southern portion of Aeolis Serpens is easily traceable in the daytime THEMIS IR mosaic. At this resolution, the landform appears to have a rounded morphology. Figure is centered at 3.2°S, 151.5°E. White box is outline of Fig. 5.

we compare the observed Aeolis Serpens morphological attributes to a potential terrestrial analog, an inverted channel that preserves the Mirackina paleoriver in South Australia. The Mirackina paleoriver has been suggested as a general analog for martian sinuous ridges (e.g., Pain and Clarke, 2009; West et al., 2010), but this study is the first to conduct a detailed comparison of this landform to a specific martian sinuous ridge. Our work strengthens the fluvial interpretation for Aeolis Serpens. We assess the applicability of paleohydrologic models to groundwater cemented inverted fluvial landforms, and we report discharge estimates for both Aeolis Serpens and Mirackina.

2. Data and methods

2.1. Image and digital terrain models

A combination of images and topographic data was analyzed to determine landform attributes. We examined ConTeXt camera (CTX, 6 m/pix; Malin et al., 2007) and High Resolution Imaging Science Experiment (HiRISE, 25 cm/pix; McEwen et al., 2007) images to identify morphological characteristics of a martian sinuous ridge. First, we visually assessed the landform morphology in CTX images (Fig. 3; Tables 1 and 2) based on eight categories of transverse shape (defined in Fig. 4). Second, we extracted topographic cross sections from CTX digital elevation models (DEMs, Figs. 5–8) to check the morphological classification determined qualitatively from the image data.

Table 1
Aeolis Serpens morphology type from visual CTX image assessment.

Section	Approximate length (km)	Type
A	28	Ridge-bounded trough
B	28	Trough, possibly ridge-bounded
C	19	Trace
D	21	Trough, possibly ridge-bounded
E	10	Rounded ridge
F	10	Shallow trough/trace
G	65	Rounded ridge
H	65	Single and double ridges
I	145	Rounded ridge and trace
J	26	Trace
K	274	Single and double ridges

Planform attributes were measured from map projected CTX images; average and standard deviation values are reported. The width of the feature was measured every ~5 km along the landform, for a total distance of 300 km. In meandering sections, sinuosity (ratio of the actual landform length to the straight line distance) and radius of curvature (radius for circle fitted to meander bend) were measured. The degree of sinuosity is commonly classified based on the following ranges: straight (1–1.05), low sinuosity (1.06–1.30), sinuous or meandering (1.31–1.8), and tortuous (>1.8), with meandering rivers defined to have sinuosity ≥ 1.3 (e.g., Schumm, 2005, p. 11; Fryirs and Brierly, 2013, pp. 183–186).

Stereo pairs from both the CTX and HiRISE instruments were used to assess the topographic landform shape. CTX DEMs were

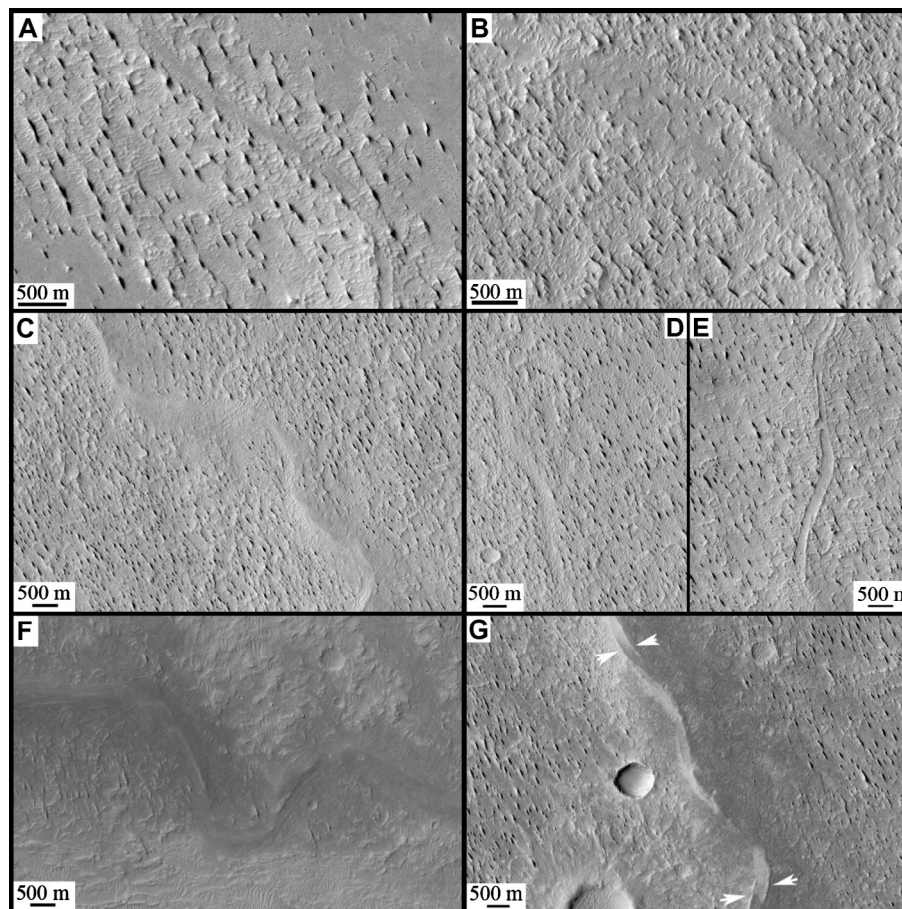


Fig. 3. Examples of Aeolis Serpens morphology types determined in CTX images. Trace and shallow trough (with aeolian bedforms in the topographic depression) are illustrated in (A) and (B). (C) and (F) illustrate examples that appear rounded. (D) and (E) are examples of troughs, where the later example appears ridge-bounded. (G) is an example of a double ridge form (white arrows). Table 2 lists the morphology section, location, and the CTX image identification for each example.

Table 2
Section, Location and CTX Image ID for Figures.

Figure	Section	Approximate location (°lat., °E lon.)	CTX ID
Fig. 3A	B	2.59, 147.64	P16_007171_1816_XI_01N212W
Fig. 3B	C	1.99, 147.92	P04_002490_1828_XI_02N212W
Fig. 3C	G	0.78, 148.60	G05_020370_1821_XN_02N211W
Fig. 3D	F	1.381, 148.27	G05_020370_1821_XN_02N211W
Fig. 3E	B	2.39, 147.70	P16_007171_1816_XI_01N212W
Fig. 3F	I	1.59, 150.04	B17_016190_1787_XN_01S209W
Fig. 3G	H	-0.19, 148.99	P14_006604_1778_XI_02S211W
Fig. 6	I	-1.59, 150.04	B17_016190_1787_XN_01S209W
Fig. 7A	K	-2.05, 150.91	B17_016335_1775_XI_02S209W
Fig. 7B	K	-2.28, 151.05	B17_016335_1775_XI_02S209W
Fig. 7C	K	-2.46, 151.14	B17_016335_1775_XI_02S209W
Fig. 7D	K	-2.76, 151.20	B17_016335_1775_XI_02S209W
Fig. 8A	K	-3.52, 151.70	B11_013790_1757_XI_04S208W
Fig. 8B	K	-3.60, 151.71	B11_013790_1757_XI_04S208W
Fig. 8C	K	-3.87, 151.84	B11_013790_1757_XI_04S208W
Fig. 8D	K	-4.23, 151.88	B11_013790_1757_XI_04S208W

generated using a version of the NASA Ames Stereo Pipeline (Broxton et al., 2011) modified by Malin Space Science Systems as detailed in Shean et al. (2011). The CTX-derived DEM has a horizontal resolution of 6 m/pixel (resolvable resolution of 18 m) and a vertical resolution of ~10 m with residual offsets of 10–30 m relative to MOLA shot elevation as is generally true from this technique (Shean et al., 2011). Unfortunately, no CTX stereo pairs currently exist for the northern half of the landform, although these data have been requested for future image opportunities.

Study of the Mirackina paleoriver in South Australia, involved examining Landsat images (30 m/pix; Chander et al., 2009) acquired in 1991 and 2003. Topographic shape was determined quantitatively from Advanced Spaceborne Thermal Emission and Reflection Radiometer (ASTER) DEM data (30 m/pix; Abrams et al., 2010). In addition, we conducted ground reconnaissance at four sites along 80 km of the Mirackina paleoriver in May 2011. We selected sites with different transverse shape (e.g., mesa, double ridge, pinnacle ridge). At each site, we made *in situ* observations of sedimentary structures, grain size, color, cementation attributes, and outcrop attributes.

2.2. Paleohydrologic reconstruction

Empirical relations derived from modern terrestrial rivers can be used to estimate aspects of the paleohydrologic flow conditions (e.g., Williams, 1984, 1988). The most useful relationships for this work are those that relate channel dimensions and/or meander planform to discharge. Following similar methodology from prior studies to reconstruct paleohydrological conditions for inverted channels (e.g., Maizels, 1987; Williams et al., 2009), we have examined the published literature for empirically derived macrorelationships for bankfull channel width, W_b , and discharge, Q , with input parameters that are potentially measurable for inverted fluvial landforms. Table 3 lists these empirically derived regression relationships, as well as the applicable range for the input parameter, correlation coefficient and standard error for each equation (an estimate of standard error was not given in Williams (1984) for Eq. (1)).

For a meandering channel pattern, bankfull channel width, W_b , can be estimated based on meander wavelength, λ , or radius of curvature, R_c . Eq. (1) is a least squares regression derived by Williams (1984) based on data for 16 rivers in the central United States reported by Dury (1976). Eqs. (2) and (3) are regressions derived from a larger dataset of rivers (>80) in a range of physiographic

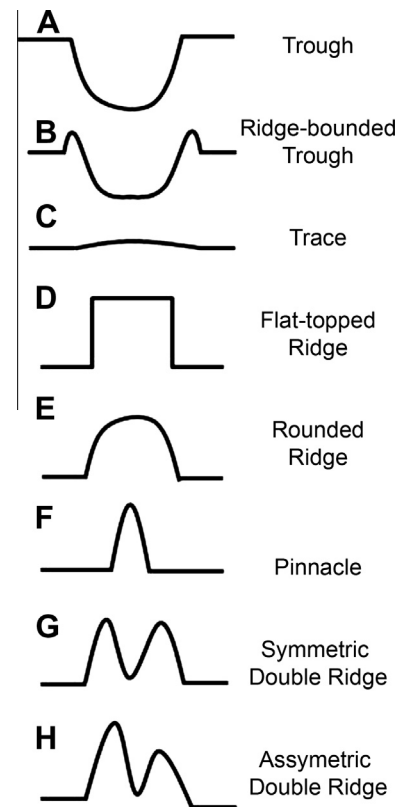


Fig. 4. Schematic illustrating variations in cross-sectional shape for rivers, ranging from original negative relief (A and B), to forms that result from erosion, such as minimal relief (C), single ridge (D–F), and double ridge types. Ridge-bounded trough is analogous to the form observed in a leveed river valley. In instances where the continuity of the landform (based on albedo, color and/or surface texture consistent with other regions of the landform) can be followed even when there is minimal relief, these reaches are classified as trace (C). Ridge-bounded trough (B) and double ridge (G and H) differ by the relative width and depth of the trough (e.g., for B, the trough is wider than the bounding ridges; for G and H, the two ridges match the width of the rest of the landform, and the intermediate trough can vary in depth and width).

environments in North America and Australia, and they apply to channels with sinuosity ≥ 1.2 (Williams, 1988).

Both average daily discharge, Q_{ave} , and channel-forming flood discharge (Q_n , where n is the recurrence interval of the channel-forming flood in years) are informative parameters (e.g., Williams, 1988; Knighton, 1998, pp. 162–167). The former provides an estimation of flow magnitude on an average day of continuous flow, and it is frequently the reported discharge value from hydraulic gauging stations. As the average discharge is a daily measure, it is sensitive to the amount of precipitation that falls within the drainage basin and ultimately feeds the river. However, higher-magnitude events are thought to govern the resultant river morphology for alluvial channels, and a number of studies have found that the dominant flood occurs with a recurrence interval of a year or two in humid regions (limitations to this relationship are discussed in Knighton (1998, pp. 162–167, 216–217)). This long-term statistical discharge also uses river gauging station data. One important caveat is that a variety of flow stages may be reflected in this value, including flow within the streambanks, bankfull flow, and overbank flow. Although we use channel-forming discharge relations based on 1.5 and 2 year recurrence intervals, no inference on the frequency of flood magnitudes is implied for these paleorivers.

Estimates of both types of discharge are from two studies on rivers within the United States. Two regression relationships (Eqs. (4) and (5)) derived by Williams (1984) based on 31 rivers

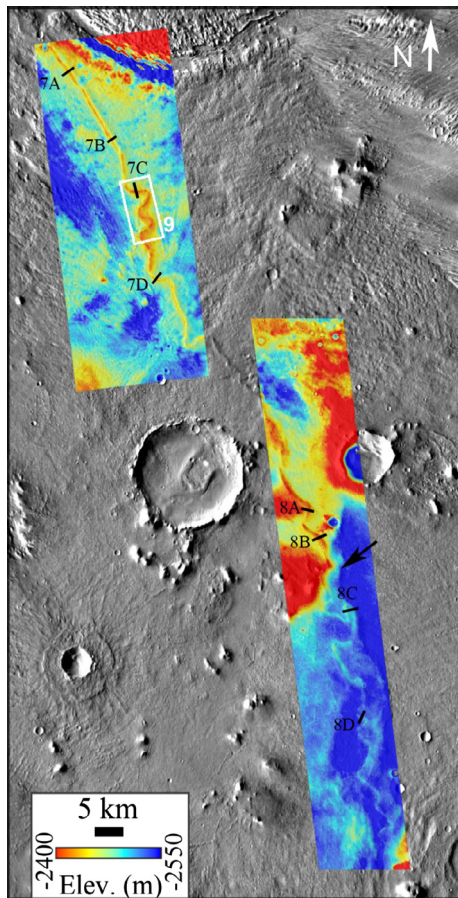


Fig. 5. Digital elevation models (DEMs) derived from CTX stereo image pairs are superposed on the THEMIS daytime infrared mosaic. The maxima associated with Aeolis Serpens undulate along course; a dramatic elevation drop (~ 100 m) over a short baseline is marked by the black arrow. White box is location of Fig. 9. Black lines mark cross-section locations shown in Figs. 7 and 8. Upper DEM is derived from images B17_016335_1775_XI_02S209W and B17_016414_1776_XN_02S208W (see Fig. 7 for illustrations). Lower DEM is derived from images B11_013790_1757_XI_04S208W and P05_003136_1746_XN_05S208W (see Fig. 8 for illustrations). Image center is at 3.3°S , 151.5°E .

in the central United States reported by Carlston (1965) relate discharge to meander wavelength. Eqs. (6) and (7) relate discharge to bankfull width, and are based on 252 rivers in the west-central United States (Osterkamp and Hedman, 1982).

Liquid flows in open channels due to the acceleration of gravity, which on Mars is 38% of the value on Earth. For a comparable stream (width, depth, slope and bed roughness) on both planets, a lower discharge is expected on Mars relative to the terrestrial counterpart. Although empirical terrestrial equations are commonly scaled for martian gravity (e.g., Komar, 1980; Moore et al., 2003; Wilson et al., 2004; Irwin et al., 2005, 2008; Burr et al., 2010), an approach that we will adopt in this study, we acknowledge that the effect of changing the gravity and shear stress may affect channel geometry relative to a given channel-forming discharge, and bank strength on Mars is unconstrained, so our paleo-discharge estimates incorporate significant sources of error. To account for the lower gravity on Mars relative to Earth, a scaling parameter (Table 1) was applied to the derived width and discharge values (see appendix B in Burr et al., 2010). The scaling factors are propagated through error analysis.

Total error for computed values (W and Q) is based on two components. First, the spread in measurements for the input parameter (meander wavelength, radius of curvature, bankfull width) is re-

ported as the standard deviation of the mean. Second, the standard error (as well as the correlation coefficient) reflects the goodness of fit for the regression Eqs. (1)–(7) to the data. The total error from these independent sources is calculated using addition in quadrature, or as the square root of the sum of the squares (Taylor, 1982, pp. 57–62). For additional details on combining these two sources of uncertainty into the total error, see Appendix C in Burr et al. (2010). The reported total error here does not include other sources of uncertainty in this approach, as discussed further in Section 4.2.

3. Observations

3.1. Aeolis Serpens

The focus of this paper is an extensive (~ 500 km long) sinuous ridge, Aeolis Serpens, located between two lobes of the MFF in the Aeolis/Zephyria Planum region of Mars (Figs. 1 and 2). At the northern extreme (3.17°S , 147.48°E), Aeolis Serpens is a twin lateral ridge with a distinct terminal escarpment, suggesting that erosion has removed the reach that extended further to the north. The southern end of Aeolis Serpens is a low relief ridge that is superposed by yardangs in places. Along course, variations in landform shape (mesa, trough, etc.) result in a range of Aeolis Serpens width values: 390 ± 120 m. The planform of Aeolis Serpens is relatively linear over much of the length. However, the southern third has a pronounced curvilinear path with a typical sinuosity of 1.4. Maximum sinuosity (1.9) is measured at the reach centered at 2.53°S , 151.16°E . Irregular meanders characterize the southern section where the radius of curvature (865 ± 275 m, $n = 9$) and wavelength (5580 ± 670 m, $n = 5$) were measured (Fig. 2).

Our results show that the cross-sectional morphology varies along course. For simplicity, we mark the junction between morphological sections as discrete points in Fig. 1; however, these locations are more accurately transition regions as the morphology rapidly varies along course and the classifications in Table 1 report the pervasive type within each section. Approximately one fifth of the Aeolis Serpens has negative or minimal relief (e.g., trace, Fig. 4), and in many places it has a double ridge shape.

Second, we extracted topographic cross sections from CTX DEMs to check the morphological classification determined qualitatively from image data (Figs. 6–8). The cross sections show the rugged nature of the surrounding landscape (typical local relief of ~ 5 m) in this wind-scoured region. In the southern portion where we have CTX DEMs, Aeolis Serpens is typically a ridge form with width that varies from 100 m (e.g., pinnacle ridge in Figs. 6D and 7B) to approximately 500 m (rounded or flat-topped ridge). In some reaches, the landform has minimal relief relative to the surroundings, and was classified as ‘trace’ (Fig. 6E and F).

The visual impression of sinuous ridge morphology based on CTX images does not always match the transverse elevation profile. Fig. 6 illustrates a short stretch that appears to have relatively consistent morphology in the CTX image where it was classified as ‘trace’, but the transverse shape varies from flat-topped ridge to pinnacle to essentially flat, and relief ranges from 0 to 20 m. This result was confirmed in three independently derived CTX stereo image pairs at this location (B17_016190_1787_XN_01S209W and P17_007606_1808_XI_00N210W Fig. 6; B17_016190_1787_XN_01S209W and P16_007105_1774_XN_02S209W; B17_016190_1787_XN_01S209W and P16_007461_1784_XI_01S210W).

Another example of critical shape information revealed from CTX DEMs is in Fig. 8C. The loop in this sinuous ridge appears to have a uniform rounded shape in the CTX image, but the cross-sectional shape varies from a narrow ridge on the western side to a lower-elevation, flat-topped ridge on the eastern side of the loop.

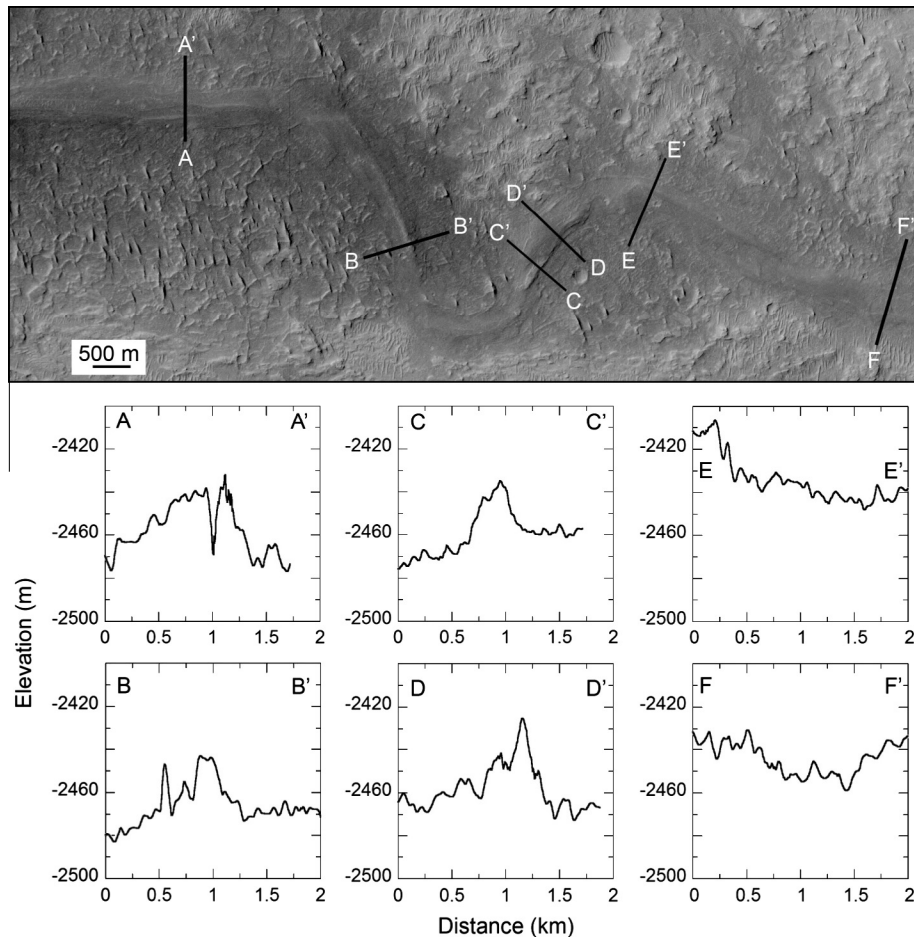


Fig. 6. Top panel: Section of Aeolis Serpens where the morphology was initially characterized as 'rounded' and 'trace' in CTX image analysis. See Table 2 for additional information. Bottom panels: Six topographic cross sections illustrate the range of shape within a short region: double ridge (A–A'), flat-topped ridge (B–B'), asymmetric double ridge (C–C'), pinnacle ridge (D–D'), and trace (E–E' and F–F'). Vertical exaggeration is 20 \times . Topographic cross sections were extracted from CTX DEM derived from images B17_016190_1787_XN_01S209W and P17_007606_1808_XL_00N210W.

This site also illustrates significant variability in the longitudinal elevation profile, as there is a dramatic decrease of ~ 40 m in the elevation maxima from the western to the eastern side of the bend.

Several reaches of Aeolis Serpens have paired lateral ridges (e.g., Figs. 3G, 7C, 8D, and 9). This form is often associated with bends in the landform path. Often the more prominent ridge is located on the inner side of the bend (Fig. 9).

The elevation of Aeolis Serpens varies along course in high-resolution CTX DEMs (Fig. 5), consistent with the analysis of Mars Orbiter Laser Altimeter data by Burr et al. (2009). Both the relief relative to the surrounding surface (range: -10 m to $+70$ m) and the longitudinal profile (ridge surface elevation) fluctuate. With the transitions in form (e.g., mesa to trace), the elevation of Aeolis Serpens typically changes a few tens of meters over short baselines of <1 km (e.g., Fig. 5 and Fig. 8C). We note one location with a significant elevation drop of 100 m (arrow in Fig. 5) which may, in part, reflect relic topography (prior to landscape inversion) as there is a prominent bench at that location.

3.2. Mirackina paleoriver

The Mirackina ridge, located north of Coober Pedy, Australia, preserves the flow path (>200 km) of a paleoriver in inverted relief (Fig. 10). The ridge was first recognized as a paleoriver in a 1972 Landsat image where the landform was easily distinguished due to the presence of iron oxide in the silcrete (ferruginized silcrete) detected in band 7 (Fig. 10A; Barnes and Pitt, 1976). Barnes and Pitt

(1976) defined the Mirackina Conglomerate, the stratigraphic unit that caps the ridge, and identified the materials as cemented fluvial sediments. The planimetric pattern of this ridge, including meandering in some reaches and a few tributary ridges, was key to identifying this landform as indurated stream deposits that had undergone topographic inversion. One ~ 20 -km reach (starting at approximately the location of cross-section 5 in Fig. 10A and extending to the northwest) has an irregular meander pathway with sinuosity of 1.3, a meander wavelength of 5060 ± 1260 m ($n = 4$) and a radius of curvature of 1060 ± 115 m ($n = 8$).

The Mirackina paleoriver channel fill deposits are surrounded by the Cretaceous Bulldog shale unit (McNally and Wilson, 1996). Paleodrainage is presumed to be Miocene in age based on stratigraphic relations (Barnes and Pitt, 1976; McNally and Wilson, 1995), but the constraint on age is weak (Hou et al., 2008). Flow direction was to the south into the ancestral Lake Eyre. The fluvial deposits of the Mirackina paleoriver were cemented and later remained preserved as a ridge when differential erosion (presumably a combination of fluvial and aeolian degradation) removed the less resistant valley walls. (In this study, we use 'channel' to refer to the conduit of flow, and distinguish this from 'valley', the larger topographic depression that includes the river channel.) The landform is extensively dissected and segmented by erosion, such that it is now defined by a line of ridges and mesas with 30–40 m of relief above the surrounding plains (Fig. 11). The modern-day flow path to Lake Eyre is via Arckaringa Creek, an ephemeral sand-bedded braided channel (Fig. 10).

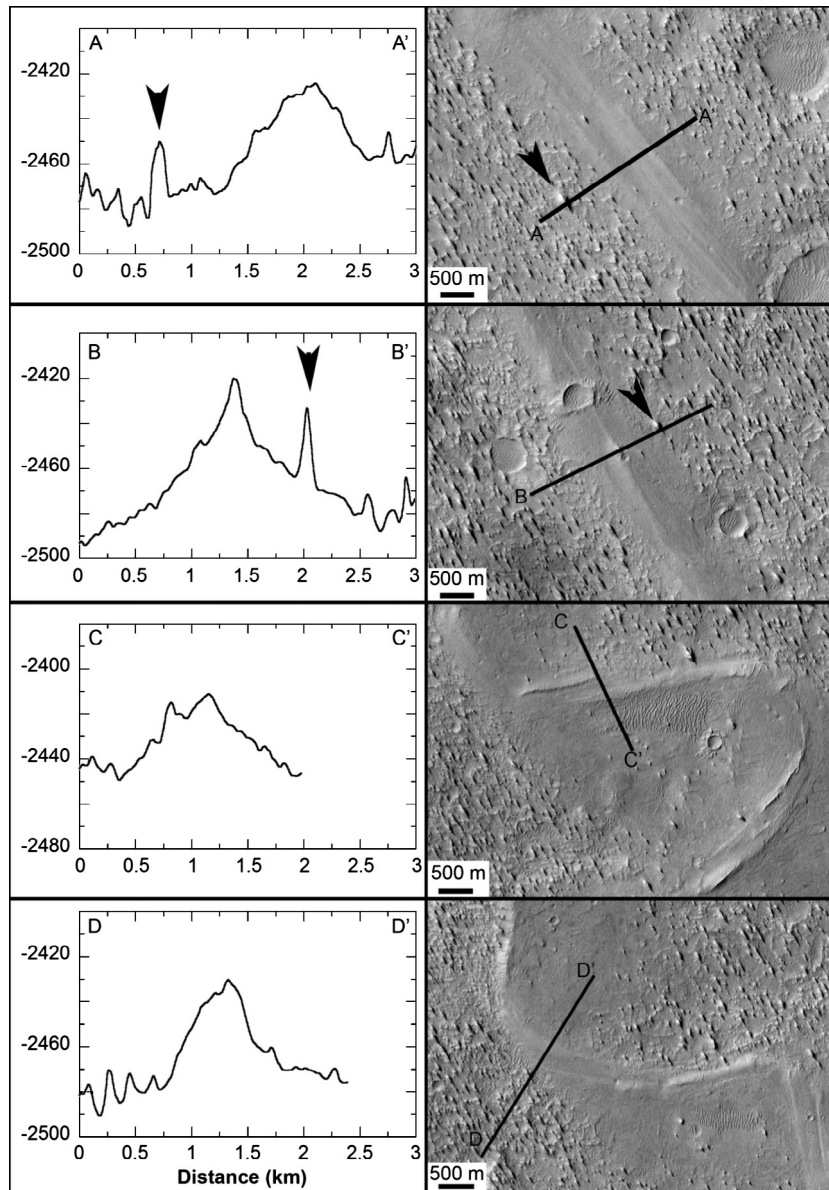


Fig. 7. Illustrations of cross-sectional shape and image morphology: rounded ridge (A–A'), pinnacle ridge (B–B'), asymmetric double ridge (C–C'), and rounded ridge (D–D'). Black arrows mark location of prominent yardangs with relief of ~20 m. Elevation scale on y-axis is in meters. Vertical exaggeration is 20×. See Table 2 for additional information and Fig. 5 for locations.

The cross-sectional shapes of the Mirackina landform include flat-topped ridge (910 ± 250 m width) and double ridge (both symmetric and asymmetric; 740 ± 130 m width) morphologies (Fig. 12). Twin lateral ridges mark the course of the Mirackina paleoriver along the majority of its length. In sinuous regions of the ridge, asymmetric paired ridges are present, and the higher ridge is present on either the inner or outer side of the bend (e.g., Fig. 12, profiles 6–8). Maximum elevation varied between the west and east side of the landform (Fig. 12), providing evidence of variable cementation of the fluvial deposits.

The Mirackina Conglomerate is subdivided into two units that are together up to 15 m thick, with typical exposures of 5–10 m (Barnes and Pitt, 1976). The upper portions of the ridges are massive, fine to medium-grained sandstone that is variably cemented by silica and iron oxides (McNally and Wilson, 1996; Barnes and Pitt, 1976; Fig. 13A and E). The caprock has a shallow dip ($<10^\circ$) inward to the former valley center (Fig. 13A). A second unit is cross-bedded, medium to coarse-grained quartz sandstone observed on vertical exposures 2–10 m from the ridge crest (Fig. 13B–D). With-

in this unit are low-angle planar cross-bedding of about 0.6 m thickness. There is tremendous variability in the character of the silicified deposits. In some places there are centimeter-sized silcrete nodules, often aligned with bedding, whereas in others masses of silcrete in the sandstone or entire blocks of material were silicified, and the original sedimentary structures were completely overprinted. These observations suggest that the cementation process was not uniform throughout the river system, and that localized cementation occurred.

4. Discussion

4.1. Formation of the Mirackina ridge

McNally and Wilson (1996) proposed a lateral groundwater discharge silicification model to explain the cementation history for the Mirackina Conglomerate (Fig. 14). They proposed that during a period of reduced precipitation during the Late Miocene to Pliocene, flow within the Mirackina was diminished and a line of

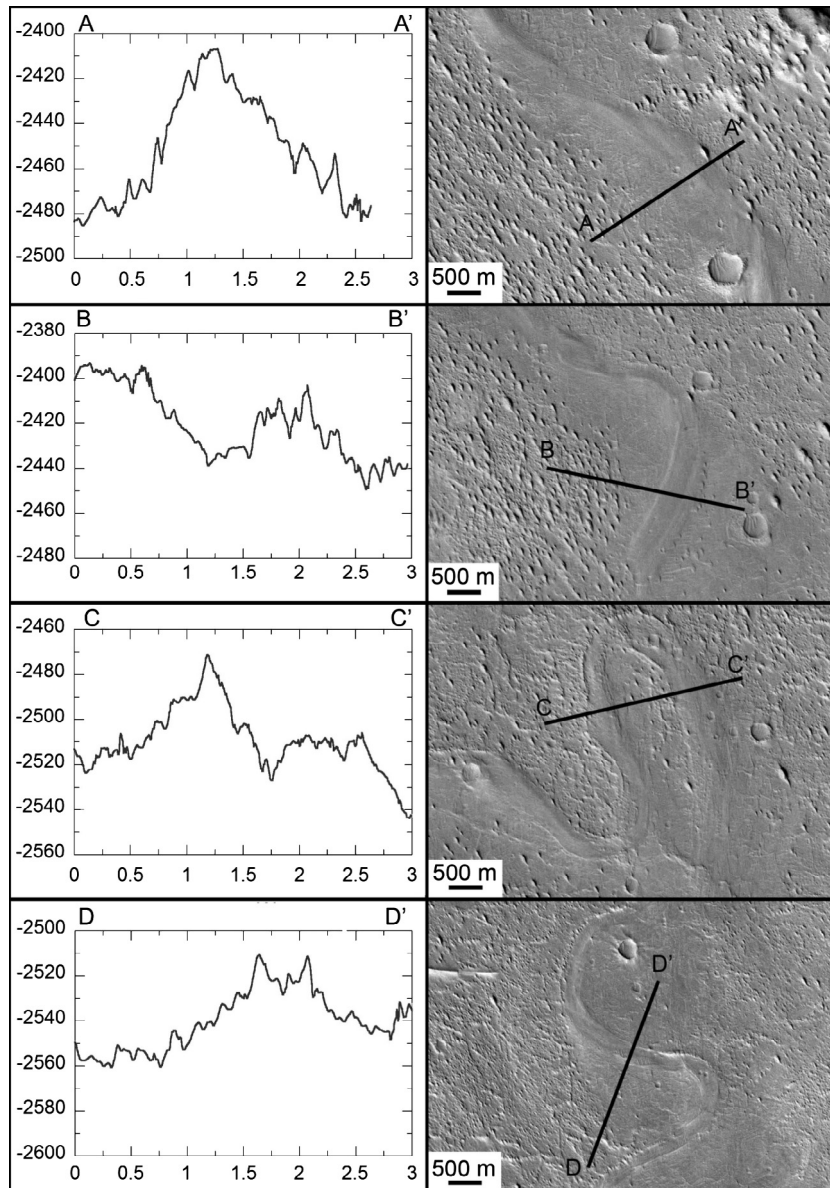


Fig. 8. Illustrations of cross-sectional shape and image morphology for Aeolis Serpens: flat-topped ridge (A–A'), asymmetric double ridge (B–B'), pinnacle (left) and flat-topped (right) ridge (C–C'), and symmetric double ridge (D–D'). Note that the landform shape changes in the loop (C–C'), although this is not readily discernible in the CTX image. Elevation scale on y-axis is in meters. Vertical exaggeration is 20 \times . See Table 2 for additional information and Fig. 5 for location.

groundwater seepage sites was present along either side of the broad alluvial channel. Silica-charged groundwater gradually entered the channel sands at the alluvium/bedrock interface. As the groundwater evaporated via capillary rise, lenses of silicified channel deposits formed that dip and thin from the valley margins toward the valley center. In this model, silicification first occurs at the valley margins as silica is removed from the groundwater and the cement thins laterally inward as the concentration of silica decreases in the groundwater. The altitude of groundwater discharge would fluctuate seasonally as the water table oscillated throughout the year, resulting in different vertical horizons that were cemented over time. Silicification may have also occurred into the Pliocene after fluvial activity in the Mirackina paleoriver ceased (thought to be in the Miocene; Barnes and Pitt, 1976; McNally and Wilson, 1996). In addition, there were likely temporal and spatial changes in groundwater chemistry. McNally and Wilson (1996) suggest that late-stage ferruginization of the silcrete caprock may be a reflection of iron-rich groundwater during a per-

iod of increased aridity in the region. They observed spatial variations in the cement chemistry and noted ferruginized silcrete is more prevalent in the northeastern rim of the Mirackina Conglomerate, as observed in the false-color Landsat image (Fig. 10A).

The variability in ridge form for the Mirackina Conglomerate is directly related to the groundwater cementation mechanism. Alluvium in the valley center typically remained weakly indurated to uncemented, and was removed by subsequent erosion after active channel flow in the Mirackina paleoriver ceased. Material at the margins was preferentially cemented, and upon landscape inversion these locations became double ridges. In rare locations, silicification of the entire valley occurred, ultimately resulting in ~ 1 km wide mesas (see cross-sections 3 and 4 in Figs. 10 and 12); thus the preserved ridge in these locations is wider than the former river channel. The spatial variability in cementation sites is a major influence on the modern landform morphology: intermittent mesas and paired ridges that outline much of the former flow path, with the silicified channel remnants dipping toward the channel

Table 3
Hydraulic regression equations.

Equation		Applicable range ^a	Correl. coeff. ^a	Std. error ^a (%)	Scaling factor	Reference
$W_b = 0.43\lambda^{0.73}$	(1)	$2.6 > \lambda > 3000$ m	0.89	–	1.25	Eq. (3) in Williams (1984)
$W_b = 0.17\lambda^{0.89}$	(2)	$8 > \lambda > 23,200$ m	0.93	47	1.25	Eq. (2) in Williams (1988)
$W_b = 0.71R_c^{0.89}$	(3)	$2.6 > R_c > 3000$ m	0.94	40	1.25	Eq. (5) in Williams (1988)
$Q_{ave} = 0.000017\lambda^{2.15}$	(4)	$145 > \lambda > 15,545$ m	0.99	26	0.63	Williams (1984)
$Q_{1.5} = 0.011\lambda^{1.54}$	(5)	$145 > \lambda > 15,545$ m	0.98	11	0.62	Williams (1984)
$Q_{ave} = 0.027W_b^{1.71}$	(6)	$0.8 > W_b > 430$ m	0.93	79	0.68	Osterkamp and Hedman (1982)
$Q_2 = 1.9W_b^{1.22}$	(7)	$0.8 > W_b > 430$ m	–	109	0.62	Osterkamp and Hedman (1982)

^a Applicable range, standard error and correlation coefficient reported in Williams (1984, 1988).

center (Fig. 14A). With the groundwater silicification model, the modern surface slope (cross-sectional) on the mesa reflects the hydraulic gradient from the point of spring discharge.

Importantly, the longitudinal profile of the Mirackina ridge does not preserve the slope of the paleoriver as the cementation had temporal variability and preferentially preserved the valley margins. By convention, a longitudinal profile is constructed by the centerline of the river to determine the down-slope gradient. However, the central Mirackina paleoriver deposits have often been removed, as these sites were less indurated and therefore more susceptible to erosion. In such a case where there is partial preservation of the landform, another approach would be to connect the remnants (in this case maximum elevations). However, this approach results in a path that veers between the downstream right and left banks (see variations in ridge maxima in Fig. 12). Along course, the topmost surface elevation typically varied by 10–15 m over baselines of 1–2.5 km (see also McNally and Wilson, 1996). In the extreme, one ~15 km reach has a ~20 m difference in maximum elevation that is counter to the paleoflow direction. These locations are interpreted to be associated with the valley margins rather than the river channel, and therefore they do not aid in determining the river gradient.

We are aware of few terrestrial inverted fluvial landforms that share the range of transverse shape and specifically the double ridge morphology of the Mirackina paleoriver. Twin lateral ridges have been identified in the Atacama Desert, Chile (see Fig. 3d of Lefort et al., 2012), although their formation mechanism is not understood. Thus, the Mirackina paleoriver is an apparently rare example that helps to illustrate one preservation style for inverted fluvial landforms and is instrumental for recognizing landforms that may have had a similar formation history on Mars.

4.2. Formation of *Aeolis Serpens*

Burr et al. (2009) favored the esker interpretation (yet retained the fluvial landform as an alternative hypothesis) for *Aeolis Serpens* on the basis of (1) the rounded cross-sectional shape, (2) isolated network morphology, and (3) the large-scale (~100 m) variations in elevation maxima along the landform. These attri-

butes are consistent with eskers, which are deposits from a stream that flowed within or beneath a glacier. Terrestrial eskers can extend over distances of >100 km, and can traverse topographic divides due to the pressurized flow that can occur within subglacial ice tunnels (e.g., Shreve, 1985; Cuffey and Paterson, 2010, p. 196). Eskers characteristically have a rounded form (e.g., Bennett and Glasser, 2010, pp. 272–278), and do not typically have a double ridge morphology as is present in *Aeolis Serpens*. Burr et al. (2009) acknowledged several potential discrepancies with an esker origin for this sinuous ridge. There is a lack of other identified glacial landforms in the region to support an esker origin. In addition, it is thought that the pronounced sinuosity (e.g., Fig. 9) is not a common attribute for eskers (Burr et al., 2009). In subsequent analysis with higher-resolution data, these three attributes in support of an esker formation were discounted (Lefort et al., 2012).

With the Mirackina example, the morphological characteristics of *Aeolis Serpens* are consistent with interpretation as an inverted fluvial landform resulting from variable cementation. A rounded or flat-topped cross-sectional shape can result from cases where the entire breadth of alluvium is cemented, as seen in the Mirackina example (e.g., Fig. 12). However, the more common expression is for single or double ridge forms resulting from sporadic cementation. Examination of CTX images of *Aeolis Serpens* revealed that the landform has a range of cross-sectional shapes including mesa, negative relief sections (troughs), and most commonly (~50% of the length) single ridge and double ridge varieties (Table 1), similar to the Mirackina example. The Mirackina paleoriver does preserve tributary segments, but they are rare and isolated from the main trunk section. Spring-fed cementation of the Mirackina channel deposits preferentially occurred or was more concentrated along the main trunk resulting in few tributary paths preserved. This pattern is similar to that observed in *Aeolis Serpens* which has a few nearby sinuous ridges in the southern reach, that may be disconnected segments of the *Aeolis Serpens* network (see also Fig. 3a in Lefort et al., 2010). Thus, it is possible that the apparent isolated network morphology of *Aeolis Serpens* may also be related to the cementation scenario. The undulations in the longitudinal profile are not a hindrance to this interpretation, as the Mirackina example illustrates that flow gradient (paleoslope) is not preserved. The



Fig. 9. HiRISE anaglyph PSP_007395_1775 and ESP_016414_1775 of a highly sinuous section of Aeolis Serpens. Paired lateral ridges are present. Image center is 2.47°S, 151.14°E.

magnitude of the elevation undulations along Aeolis Serpens (typically a few tens of meters over baselines of <1 km) is generally consistent with that observed in the Mirackina example, an indication of the plausibility of a differential cementation mechanism to produce this relief variation. Comparable vertical offsets for other sinuous ridges in this region were similarly attributed to heterogeneous cementation and erosion by Lefort et al. (2012).

Aeolis Serpens has attributes in common with terrestrial meandering rivers. Meandering rivers are characterized by the sinuous course of the channel, with sinuosity values of ≥ 1.3 (e.g., Schumm, 2005, p. 11; Fryirs and Brierly, 2013, pp. 183–186), a criteria met in reaches by both the Mirackina paleoriver and Aeolis Serpens. In an unconfined valley setting, the lateral stability of meandering rivers is based primarily on the nature of the floor sediment (e.g., Fryirs and Brierly, 2013, pp. 183–186). Active meandering systems typically have a prominent gravel and/or sand bedload fraction and adjust laterally by bend migration processes. The result is a wide range of geomorphic expression such as ridges and swales, aban-

doned channels, chute or neck cut-off channels and levees (overbank deposits). In contrast, passive meandering systems are dominantly suspended-load rivers (Fryirs and Brierly, 2013, pp. 183–186). The cohesive nature of the banks promotes channel stability and limited lateral migration. Vertical accretion processes dominate and tend to create relatively flat-topped floodplains. In both of the landforms described in this work (Mirackina paleoriver and Aeolis Serpens), there is a lack of preserved geomorphic evidence indicating lateral migration of meanders, suggesting that these may have been passive meandering systems.

Flow direction for Aeolis Serpens is uncertain. In the southern reach, nearby sinuous ridges in the southern extent were mapped as potential tributaries by Lefort et al. (2012; their Fig. 3a), implying a northward flow. However, the pronounced sinuosity of these sinuous ridges could alternatively be interpreted as meandering distributaries with flow to the south if they were once connected to Aeolis Serpens.

Absent ground-based observations, the exact mechanism of the proposed variable cementation in Aeolis Serpens is not clear. Even though we have compared Aeolis Serpens to a morphological analog on Earth with cementation from point sources along its length, it is difficult to reconcile the uniqueness of this feature and its extensive scale with a spring cementation scenario in Aeolis Dorsa. No additional corroborating evidence for spring activity in this region has been identified (e.g., spring mounds, theater-headed valleys without overland sources, hydrothermal spring morphology or mineralogy). A spring system spanning many hundreds of kilometers, and apparently uniquely associated with this feature, is unlikely.

Rather than localized cementation sites, we speculate that the strength of cementation varied along course. This scenario would explain the extensive continuity of Aeolis Serpens. The principal variable may have been water chemistry, which would be influenced by the local materials over which it flowed. Thus, the concentration of various solutes may have been higher in certain reaches, ultimately leading to differences in cementation strength by location. Cementation may also have been influenced by factors within the fluvial system that promote direct precipitation, such as localized ponding or quiescent reaches. Along meandering reaches, cementation would likely first favor the inner bend which are zones of deposition, as opposed to the outer bank, which is an active zone of erosion, if the cementation occurred contemporaneously with active flow conditions. This pattern is observed in sections of Aeolis Serpens where the inner bank is preferentially preserved (e.g., Fig. 9). Heterogeneous cementation could also result from regional variations in that permeability of the substrate, a scenario that may be consistent (depending on timing) with the groundwater upwelling model proposed by Andrews-Hanna and Lewis (2011), Andrews-Hanna et al. (2007, 2010).

A potential alternative explanation for the double ridge morphology in a fluvial system is the preservation of coarse-grained channel levees. In such a case, preferential preservation would be due to overbank deposition of coarse material that would inhibit deflation. Along straight reaches, these alluvial lags could form twin lateral ridges. In curved reaches, alluvial lags would be deposited on the outer bends. This clast armoring could be a secondary form of induration that occurred at Aeolis Serpens, although we note the pattern of ridges associated with meander reaches (e.g., Fig. 9) differs from that predicted from this mechanism.

Based on new observations of the Aeolis Serpens and knowledge from the Mirackina paleoriver analog, we favor interpretation of this sinuous ridge as an inverted fluvial landform consistent with the inferred fluvial origin of other Aeolis Dorsa sinuous ridge networks (Burr et al., 2009). This revised interpretation obviates the need for special circumstances for this one example and is consistent with the lack of other glaciogenic features in the region. We

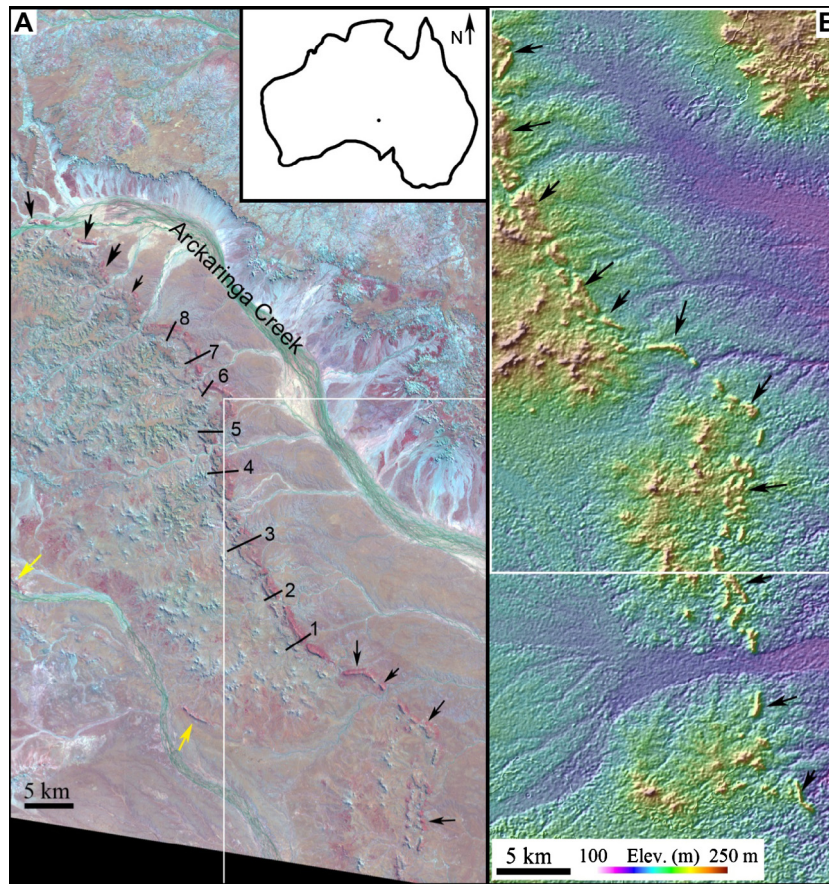


Fig. 10. (A) Mesas and ridges that define the Mirackina paleoriver appear red in this false-color Landsat image (p101r79) acquired in 1991 with bands 7–4–2 displayed as red, green and blue, respectively. Mesas in the northern and southern extent are marked by black arrows. Yellow arrows point to isolated ridges that mark former tributary paths as determined by mapping conducted by Barnes and Pitt (1976). Cross section locations (1–8) correspond to profiles shown in Fig. 12. Image center is near 27.90°S, 134.63°E. Inset shows the location of the study site relative to the Australian continent. (B) False-color digital elevation model from ASTER data. White box matches region in panels A and B. ASTER data was obtained from <https://lpdaac.usgs.gov/products/>. (For interpretation of the references to color in this figure legend, the reader is referred to the web version of this article.)



Fig. 11. (A) View (looking to the west) of Mirackina ridge from the Oodnadatta Track north of Coober Pedy. Landform is near 28.38°S, 134.84°E. Background width is ~4 km. (B) View to the southwest of Mirackina ridges, Landform is near 28.02°S, 134.67°E. Background width is ~2 km.

note that with this fluvial interpretation for Aeolis Serpens, it is one of the longest features of this type on Mars; for comparison, ~90% of martian valley networks are <200 km in length (Carr, 1996, pp. 75–76).

4.3. Paleohydraulic reconstruction of the Mirackina paleoriver

Aspects of ancient river channels are preserved in three cases: as abandoned channels on the landscape, in vertical exposures of rock outcrop (e.g., channel lenses), and rarely as exhumed or in-

verted fluvial materials. As discussed by Williams (1984, 1988), it is not straightforward to make paleofluvial estimates for paleochannels based on existing hydraulic or morphologic equations derived from modern rivers. One particular shortcoming is that many of these equations rely on measurements of active flow conditions, such as discharge or cross-sectional flow area, and these parameters are used as the independent (given) parameters. Also, the majority of hydrologic models for terrestrial rivers use slope and channel width as key inputs, two parameters that may not be well-preserved or accurately determined for paleochannels (for example due to subsequent degradation or tilting). In addition, most empirical relationships are based on a limited number of observations and are particularly applicable to rivers of the same channel pattern and a similar physiographic and climatic setting. In the case of paleohydraulic reconstruction, there is often little *a priori* knowledge of the paleoriver system, and this dearth of knowledge is part of the motivation for determining information on flow conditions from modeling. However, there is tremendous potential to derive inaccurate information about the paleofluvial conditions.

Large uncertainty in the paleofluvial input data increases the error associated with paleohydraulic estimates. There are a range of factors that can result in inaccurate input values. Burial, compaction, and tectonism can alter paleochannels resulting in measurements that do not reflect the original flow conditions. Lateral migration of streams before burial or retreat of the caprock after

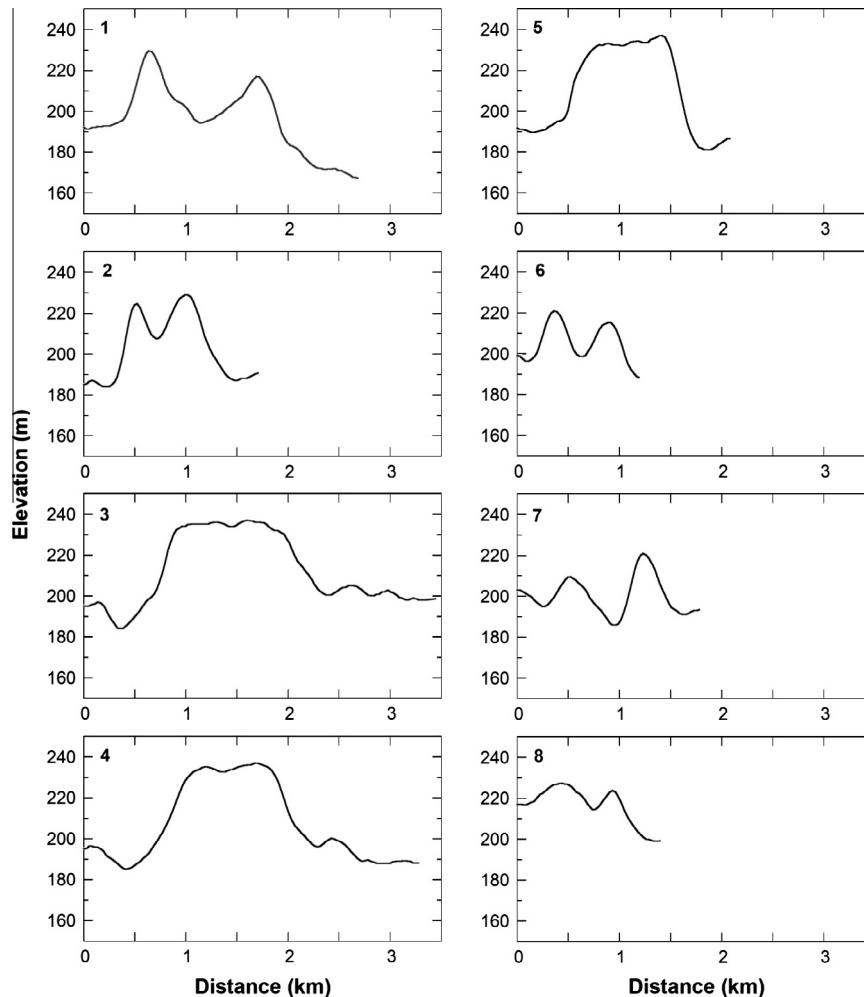


Fig. 12. Topographic cross-sections (from west to east, left to right) derived from ASTER data (see locations on Fig. 10). Shape types are as follows: (1) asymmetric double ridge, (2) symmetric double ridge, (3–5) flat-topped ridge, and (6–8) asymmetric double ridge. Vertical exaggeration is 20 \times .

landscape inversion can result in ridge width that is greater or less than the original channel width, respectively, but the meander geometry should be preserved.

The indurating mechanism can profoundly affect the preserved morphology of inverted fluvial landforms. Burr et al. (2010) illustrated some of the differences in morphology that result from various formation mechanisms (lava capping, gravel-armoring and cementation). Here, we expand upon the specific implications of cemented inverted channels for paleohydraulic reconstruction. We have identified macro-regression relationships based on potentially measureable parameters for inverted fluvial landforms (Table 1). A similar approach was employed in studies of inverted fluvial landforms in, for example, Oman (Maizels, 1987) and Utah (Harris, 1980; Williams et al., 2009). For inverted fluvial landforms, aspects of the paleochannel cross-sectional (width) and planform attributes (sinuosity, meander wavelength, radius of curvature) can be measured, but an assessment of these measurements based on the preservation history must be made before applying paleohydraulic models.

The Mirackina example illustrates some of the specific effects of heterogeneous cementation on the preserved morphology and ultimately the measured parameters. Cementation can vary both spatially (point sources) and temporally (seasonally), resulting in discontinuous preservation of the original landform and preferential preservation of the valley margins. The key attributes of flow gradient (see Section 4.2) and channel width are not well con-

strained from this type of cemented inverted landform. Mesa width likely approximates the original valley width rather than the channel flow width. In the case of double-ridge morphologies, the trough width provides an upper bound value for channel width. Two additional parameters that are preserved for the Mirackina paleoriver are meander wavelength, λ , and radius of curvature, R_c . However, only a short reach of the Mirackina landform exhibits a meandering course, so use of these parameters may not be appropriate for characterizing the former fluvial environment. In addition, the measured wavelength for the Mirackina may overestimate the channel wavelength resulting in an overestimation for paleodischarge (e.g., Dury, 1985). With these limitations and caveats in mind, we provide order of magnitude estimates of bankfull channel width and paleodischarge.

In meandering systems, terrestrial empirical relationships can be used as a check on the interpretation of the preserved landform width (i.e. is the measured width greater than, equal to, or less than the expected channel width based on meander geometry?), as was done, for example, in Burr et al. (2010). Using the equations listed in Table 3 and the average measured input parameters yields bankfull channel width values of 220–350 m (Table 4), significantly less than the measured width of the Mirackina flat-topped (910 \pm 250 m) and double ridge (740 \pm 130 m) morphologies. This discrepancy supports the interpretation that valley margins (the proposed focus point for cementation, Fig. 14) rather than channel margins are preserved here. (It is possible that cementation could

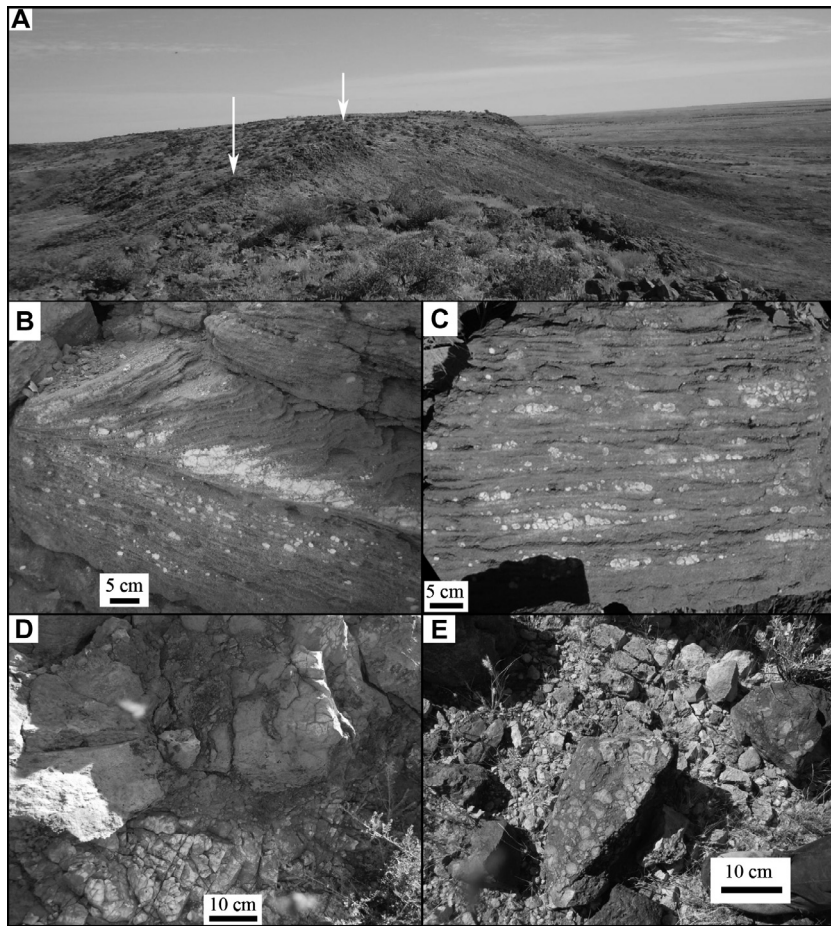


Fig. 13. (A) Silcrete caprock of the Mirackina ridge dips (e.g., between arrows) towards former valley center (left in this image). Ridge is approximately 100 m wide. Photo was taken to the northwest near 28.075°S, 134.749°E. (B–E) Examples of silicified sandstone of the Mirackina Conglomerate. Centimeter-scale silcrete nodules are aligned with bedding in (B) and (C). Massive silcrete can overprint sedimentary structures, such as the cross-bedding in (B). (D) Outcrop of massive silcrete. (E) Ferruginized block on mesa surface had silcrete nodules that were typically 5–8 cm in the longest dimension.

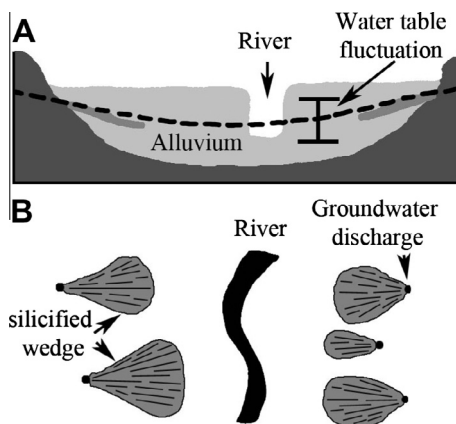


Fig. 14. Schematic to illustrate the groundwater silicification model proposed by McNally and Wilson (1996) for the development of the Mirackina paleoriver landforms in South Australia. (A) Cross-section view at the time of active river flow, presumably in the Miocene. Alluvial channel deposits (light grey) are surrounded by bedrock (Bulldog Shale, dark grey). Silicification (medium grey) occurs in wedges along the valley margin as silica-charged groundwater evaporates. The water table, shown by dashed black line, fluctuates with the seasons. (B) Plan-view of exposed silicified fans after erosion (Late Tertiary). The figure illustrates the resulting silicified fans from multiple point sources for groundwater discharge along the valley margins. Black stripe in center represents the river. Figure adapted from McNally and Wilson (1996).

also occur at points between the valley margin and channel margin, thus the preserved width could underestimate the full valley extent.) Additional support for this interpretation stems from well established meander geometry relationships from a range of fluvial environments. Meander wavelength and radius of curvature are respectively 10–14 and 2–3 times the channel width (Knighton, 1998, p. 215). Using the computed channel width in these relationships yields values that match well the measured wavelength and radius of curvature, whereas adopting the average measured Mirackina width (810 m) overestimates these two parameters by roughly a factor of 2. We adopt the larger estimate of bankfull channel width derived from Eq. (3) in computing paleodischarge, recognizing that this value is uncertain.

Average daily discharge and channel-forming flood estimates can be made based on meander wavelength and the estimated channel bankfull width. (Note that Eqs. (6) and (7) are only applicable for widths up to 430 m, consistent with the estimated bankfull width values but not the larger measured Mirackina landform width.) There is poor agreement in the two estimates for Q_{ave} and Q_n (Eqs. (4), (6), (5), and (7), respectively) reflecting the difference in the two approaches (Table 4). In both cases, the larger paleodischarge values were derived from equations based on wavelength (Eqs. (4) and (5)) rather than on bankfull channel width (Eqs. (6) and (7)).

Little insight can be gleaned from modern rivers in the region due to differences in the climatic setting and watershed geometry

Table 4
Estimated bankfull width and discharge for the Mirackina paleoriver, Australia.

Input variable	Computed parameter	Computed value	Total error	Eq.
Average wavelength	W_b	220 m	–	(1)
Average wavelength	W_b	340 m	180	(2)
Average Radius Curvature	W_b	350 m	145	(3)
Average wavelength	Q_{ave}	1565 m ³ /s	580	(4)
Average wavelength	$Q_{1.5}$	5570 m ³ /s	2730	(5)
Estimated width from Eq. (3)	Q_{ave}	605 m ³ /s	540	(6)
Estimated width from Eq. (3)	Q_2	2410 m ³ /s	2795	(7)

since the Miocene, and the lack of stream gauges on rivers and creeks. The modern climate is more arid than the presumed formation time for the Mirackina (Miocene). Arkaringa Creek, located adjacent to the Mirackina paleoriver (Fig. 10A), is an ephemeral, braided stream with a sand-filled channel. It is comparable in size to the Mirackina, but it has no meandering reaches. Floods occur within the Arkaringa Creek associated with rare, high-magnitude storm events. For example, in early February 2011 the nearby Arkaringa Station recorded 167 mm of rain over ~80 h associated with the aftermath of Cyclone Yasi (Cooper Pedy Regional Times, 2011).

In summary, paleohydraulic reconstruction of the Mirackina paleoriver provides only a general sense of the former fluvial environment. The preserved form appears to reflect a passive meandering system. Measurements of the Mirackina paleoriver meander geometry appear to be reliable dimensions of paleoflow geometry, and these metrics can be used to constrain channel width. However, direct measurement of the Mirackina paleoriver landform does not yield an accurate value for channel gradient. Based on assessment of reliable input parameters, average discharge values for the Mirackina paleoriver were likely on the order of 10³ m³/s, and formative discharges were several times larger.

4.4. Significance of Aeolis Serpens in the Aeolis Dorsa

Aeolis Serpens is one of a cluster of sinuous ridges located between the two western-most lobes of the Medusae Fossae Formation (MFF) in the Aeolis Dorsa (Burr et al., 2009). The MFF deposits are hypothesized as analogous to ignimbrites (e.g., Scott and Tanaka, 1982, 1986; Zimbleman et al. 1997; Mandt et al., 2008). (See Mandt et al. (2008) for a discussion of proposed alternate origins for the MFF. The authors conclude that the ignimbrite hypothesis matches well all of the major observations with a single mechanism, while alternate explanations require a more complex formation history.) Radar observations of the MFF indicate a dry and high porosity material (Watters et al., 2007; Carter et al., 2009). Groundwater could easily migrate through the porous MFF substrate. Fluvial activity and groundwater cementation would concentrate at low elevation. Thus, the geologic setting is consistent with the inferred formation mechanism for Aeolis Serpens presented in this work.

The MFF is particularly susceptible to erosion, suggesting that the formation is weakly indurated; aeolian deflation has resulted in the scoured landscape with yardang fields observed today. An erosional window has exposed the Aeolis Dorsa sinuous ridges, and additional sinuous ridges are inferred to be buried within the central and eastern MFF (Burr et al., 2009; Zimbleman and Griffin, 2010). Aeolis Serpens is within the lower member of the MFF, which has experienced extensive aeolian degradation. Zimbleman and Griffin (2010) estimate that a minimum of ~19,000 km³ of material has been removed from the lower member of the MFF. Aeolis Serpens was likely buried in places by younger MFF deposits and exhumed by wind erosion.

Recent mapping of the northwestern quadrant of the Aeolis Mars Chart (MC-23) has identified outliers of MFF deposits not previously recognized (Zimbleman and Griffin, 2010; Zimbleman and Scheidt, 2012). In this region, the lower member of the MFF is subdivided into two subunits, an upper Aml2 and lower AHml1 with crater retention ages (reflective of surface exposure ages) of ~3.4 Ga and ~3.6 Ga, respectively (Zimbleman and Scheidt, 2012). Superposition relationships indicate that emplacement of the lower MFF member occurred before the late Hesperian (Zimbleman and Scheidt, 2012).

For a small reach, Aeolis Serpens clearly superposes a swath of the uppermost component of the MFF lower member (Aml2; Fig. 15). CTX images and DEMs show that Aeolis Serpens is located in a local topographic low and is continuous across the mapped boundary. Based on this relationship, we infer that channelized flow in Aeolis Serpens may have occurred during the emplacement period for the lower unit of the MFF. At least portions of the landform were likely buried by MFF material, and aeolian deflation exposed Aeolis Serpens, perhaps in the early Amazonian. However, we recognize that age-dating of martian surfaces based on crater statistics is subject to question due to the combined effects of burial and exhumation (e.g., Greeley et al., 2001; Malin and Edgett, 2000a), as well as efficient secondary production (McEwen et al., 2005). Nevertheless, the relative sequence of events outlined here is robust.

Within the group of sinuous ridges at Aeolis Dorsa, Aeolis Serpens is most notable for its extensive length. Flat sinuous ridges, representing ~1/3 of the sinuous ridges in the region, are wider (>1 km) than Aeolis Serpens (Burr et al., 2009). Not surprisingly, thin sinuous ridges, classified in ~1/3 of the Aeolis Dorsa sinuous ridges, are smaller in terms of both width (65–106 m) and wavelength (685–2570 m; Burr et al., 2009, 2010). The southern extent of this landform has a meandering course, which contrasts with the generally linear path of most Aeolis Dorsa sinuous ridges; a few multi-level sinuous ridges have sinuosity values between 1.5 and 2.0 (Burr et al., 2010). Sinuous ridges in the Aeolis Dorsa occur over a range of elevations between –1700 m and –2500 m (Burr et al., 2009). Aeolis Serpens is present at the lower elevation levels (Fig. 5), and it likely formed early in the emplacement of the MFF.

As an exercise, we applied the same empirical models (Table 3) to Aeolis Serpens (Table 5), but we recognize the limitations of paleohydraulic reconstruction and the added uncertainty in applying terrestrially derived relations to Mars. (The empirical relationships used in this study are not applicable to ice-covered rivers, a possibility for aqueous flows on Mars, e.g., Carr, 1983.) Interestingly, scaled estimates for bankfull width are consistent with the measured width for the landform. This result, coupled with the relatively consistent landform width over several hundred kilometers, suggests the measured width approximates the former flow width during high-magnitude events. It also implies that cementation occurred at the channel margins or that martian wind could not move the channel-bed particles. As in the Mirackina paleoriver example, there is a disparity in the computed paleodischarge derived from the different techniques for Aeolis Serpens. Discharge estimates are greater in magnitude for Aeolis Serpens than for the thin sinuous ridges reported in Burr et al. (2010); computed average discharge in this study was between 5 and 93 times larger, while flood discharge ranged from 3 to 17 times greater. This result is not surprising as discharge scales with width and wavelength, which are both larger for Aeolis Serpens than the thin sinuous ridges in Aeolis Dorsa.

The large majority of Aeolis Dorsa sinuous ridges are interpreted as inverted fluvial landforms that formed during emplacement of the lower and middle members of the MFF (Burr et al., 2009). Orographic precipitation, either rain or snow, is believed to be responsible for the spatial distribution of sinuous ridges in

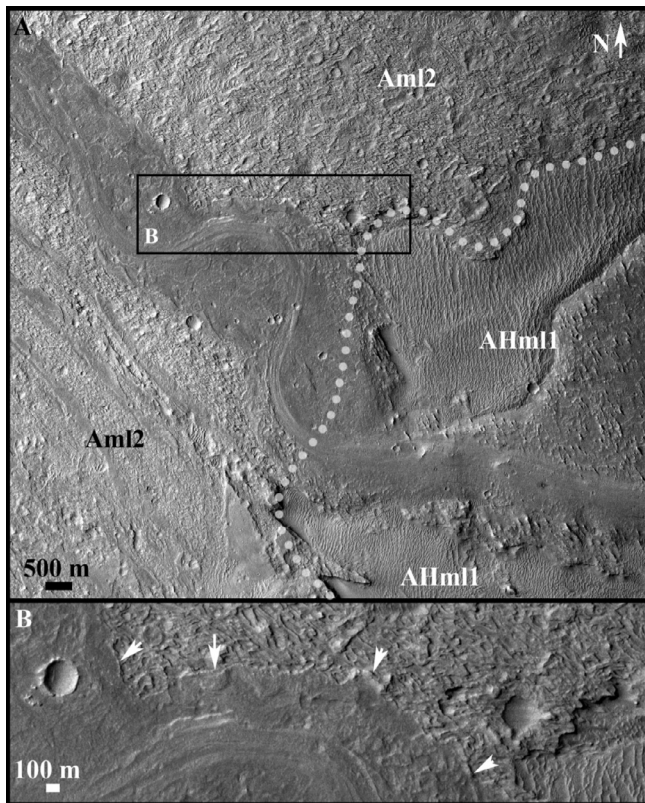


Fig. 15. (A) Sinuous section of Aeolis Serpens where it crosses lower members of the Medusae Fossae Formation as mapped by Zimelman and Scheidt (2012). Dashed line is the approximate contact between older AHm1 and younger Aml2. Image center is near 1.76°S, 150.50°E. B) Enlargement of area marked by box in panel A. Arrows point to escarpment at the edge of Aeolis Serpens, showing superposition relationship with Aml2 terrain contact. CTX image P16_007105_1774_XN_02S209W.

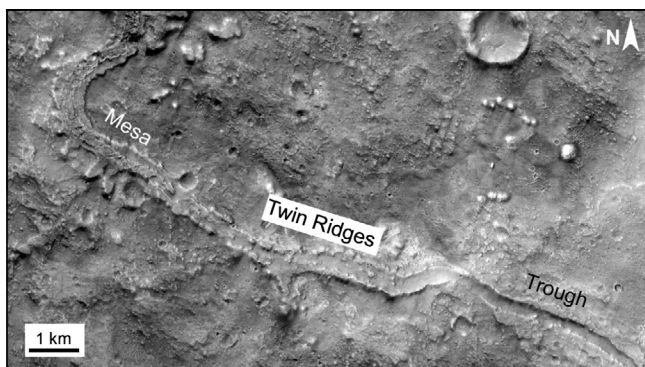


Fig. 16. Illustration of a twin-ridge landform on Mars. This example has continuity with a negative-relief trough and flat-topped mesa sections. Image center is near 10.04°N, 355.13°E. CTX image P18_008139_1900_XN_10N004W.

the Aeolis Dorsa, and particularly for the development of branched and sub-parallel network morphologies (Burr et al., 2009). Formation of Aeolis Serpens required a period of climate conditions conducive to surface runoff over great distances. Based on the stratigraphic relationships presented here, Aeolis Serpens formed early in the emplacement of the MFF, perhaps before the late Hesperian. Further study comparing the Aeolis Serpens to other Aeolis Dorsa sinuous ridges may help to elucidate temporal changes in the fluvial and climatic environment.

Table 5
Estimated bankfull width and discharge for Aeolis Serpens, Mars.

Parameter	Computed value ^a	Total error	Eq.
W_b	NA	–	(1)
W_b	370 m [460]	180	(2)
W_b	290 m [365]	150	(3)
Q_{ave}	1215 m ³ /s	350	(4)
$Q_{1.5}$	4015 m ³ /s	1725	(5)
Q_{ave}	495 m ³ /s	520	(6)
Q_2	1710 m ³ /s	1930	(7)

^a Values in square brackets are computed width values scaled for martian gravity by a factor of 1.25.

4.5. Variability in preservation of fluvial landforms on Mars

The aqueous history of Mars is based largely on the recognition of a number of landforms that indicate surface overland flow of water, including valley networks and outflow channels (Mars Channel Working Group, 1983; Carr, 1996, pp. 47–99), and gullies (e.g., Malin and Edgett, 2000b). Mars has experienced periods of burial and exhumation (e.g., Malin and Edgett, 2000a) resulting in a complex landscape, including regional topographic inversion. Therefore, preservation of fluvial landforms on Mars has a continuum of expressions. The recognition of these different preservation states and correctly interpreting these landforms is of paramount importance to documenting the history of water on Mars and assessing associated climatic conditions.

The criteria to identify cemented inverted fluvial landforms are non-unique. Collective observations that support this interpretation include geologic setting, planimetric form, continuity relationships (particularly with other recognized fluvial landforms), cement spectral signature (e.g., hydrated silica, ferricrete, sulfates, salts), and morphology. In this study, we documented a terrestrial analog of an inverted fluvial landform with heterogeneous groundwater cementation that resulted in variable morphology, and the attributes of this feature may be useful in identifying candidate cemented inverted fluvial landforms on Mars in remotely sensed data. In particular, the recognition of paired ridges may bolster the interpretation of a landform as an inverted fluvial landform, and suggest may a cementation induration mechanism.

We have conducted a rudimentary search through our existing database of sinuous ridges (Williams, 2007) and identified several with paired ridges. An example in Arabia Terra has variable morphology with transitions from trough to double ridge to flat-topped while maintaining a constant width (Fig. 16). With the Mirackina paleoriver example, the landform in Fig. 16 can plausibly be interpreted as variations in preservation of a fluvial channel along course. In this martian example, landscape inversion has only affected a portion of the valley network. Moving from right to left across the scene transitions across an erosional horizon; in this interpretation there is a ‘pristine,’ minimally eroded section (trough), a mid-section that preserves the channel margins (twin ridges), and ultimately an inverted channel (mesa). Future examination of other martian sinuous ridge sites will benefit from the morphological characteristics documented in this study.

5. Concluding remarks

New high-resolution image and topographic data reveals considerable landform variability for an extensive sinuous ridge, Aeolis Serpens, in the Aeolis Dorsa region of Mars. Although an earlier study classified this landform as a ‘rounded’ sinuous ridge, the present study documents transitions along the landform between a number of forms including trough, trace, single ridge and double ridge morphologies. Through comparison with a terrestrial analog

site, the Mirackina paleoriver in South Australia, we have reassessed the interpretation that this could be an esker in favor of the hypothesis that it could be an inverted fluvial landform. This hypothesis is consistent with (1) the newly recognized morphology presented here, (2) prior analysis of other sinuous ridges in the region (Burr et al., 2010; Zimbelman and Griffin, 2010), and (3) a recent reinterpretation of this feature (Lefort et al., 2012). We propose that the collective morphological attributes of Aeolis Serpens are consistent with variable cementation. Aeolis Serpens preserves flow conditions, with estimated paleodischarge of 10^2 – 10^3 m³/s, from an early period in the development of the MFF. The multi-hundred-kilometer flow length of Aeolis Serpens indicates that climate must have differed from present conditions at the time of fluvial activity.

Another result of this study is recognition that the induration agent has a significant impact on the resultant morphology of inverted fluvial landforms; it is critical that the formation history be correctly identified before attempting paleohydrologic reconstruction. In fluvial environments, heterogeneous cementation can partially preserve the former flow pathway. Upon landscape inversion, the resultant landform has variable shape and can transition between mesa and ridges. For cemented inverted fluvial landforms, meander wavelength and radius of curvature can be reliably measured, but flow width and gradient may not be preserved or accurately determined. Therefore, the number of applicable paleohydrologic models is restricted and only first order estimates of flow magnitude can be made. The presence of double ridge transverse shape can be instrumental in identifying potential inverted fluvial landforms on Mars.

Acknowledgments

We thank Patrick and Stephanie Williams for generously granting access to portions of the Mirackina paleoriver located on Mount Barry Station, Dr. Cliff Ollier (University of Western Australia) for valuable discussions on silcrete and ferricrete formation, David Shean (University of Washington) for software contributions and discussion of CTX DEM products, Frank Chuang (PSI) for assistance with Landsat and ASTER data for the Mirackina site, and Dr. Alexandra Lefort (University of Tennessee) for discussion of Aeolis Dorsa sinuous ridges. We thank Jim Zimbelman and Edwin Kite for their careful review of this manuscript. This material is based upon work supported by the National Aeronautics and Space Administration through the Mars Fundamental Research Program for investigation of the Mirackina paleoriver (Grant NNX06AB21G, Principal Investigator Williams), and the Mars Data Analysis Program for investigation of the Aeolis Dorsa sinuous ridge (Grant NNX08AK97G, Principal Investigator Williams, and grant NNX08BA24G, Principal Investigator Burr). This is PSI contribution #602.

References

- Abrams, M., Bailey, B., Tsu, H., Hat, M., 2010. The ASTER global DEM. *Photogr. Eng. Rem. Sens.* 76, 344–348.
- Anderson, R.B., Bell, J.F., 2010. Geologic mapping and characterization of Gale Crater and implications for its potential as a Mars Science Laboratory landing site. *Mars* 5, 76–128. <http://dx.doi.org/10.1555/mars.2010.0004>.
- Andrews-Hanna, J., Lewis, K.W., 2011. Early Mars hydrology: 2. Hydrological evolution in the Noachian and Hesperian epochs. *J. Geophys. Res.* 116, 20.
- Andrews-Hanna, J.C., et al., 2010. Early Mars hydrology: Meridiani playa deposits and the sedimentary record of Arabia Terra. *Journal of Geophysical Research.* 115, 22 pages. <http://dx.doi.org/10.1029/2009JE003485>.
- Andrews-Hanna, J.C., Phillips, R.J., Zuber, M., 2007. Meridiani Planum and the global hydrology of Mars. *Nature* 446, 163–166.
- Banks, M.E. et al., 2009. An Analysis of the Sinuous Ridges in the Southern Argyle Planitia, Mars using HiRISE and CTX Images and MOLA data. *J. Geophys. Res.* 114, E09003. <http://dx.doi.org/10.1029/2008JE003244>.
- Barnes, L.C., Pitt, G.M., 1976. The Mirackina Conglomerate. *Q. Geol. Notes Geol. Surv. South Aust.* 59, 2–6.
- Bennett, M., Glasser, N., 2010. *Glacial Geology: Ice Sheets and Landforms*, second ed. Wiley, West Sussex, 400pp.
- Broxton, M.J., Beyer, R.A., Moratto, Z., Lundy, M., Husman, K., 2011. The Ames Stereo Pipeline: NASA's Open Source Automated Stereogrammetry Software (A Part of the NASA NeoGeography Toolkit) Version 1.0.5. Published by the Intelligent Robotics Group, NASA Ames Research Center. <http://byss.arc.nasa.gov/stereopipeline/asp_book_v1.0.0alpha.pdf> (accessed 28.03.12).
- Burr, D.M., Enga, M.T., Williams, R.M.E., Zimbelman, J.R., Howard, A.D., Brennand, T.A., 2009. Pervasive aqueous paleoflow features in the Aeolis/Zephyria Plana region, Mars. *Icarus* 200, 52–76. <http://dx.doi.org/10.1016/j.icarus.2008.10.014>.
- Burr, D.M., Williams, R.M.E., Chojnacki, M., Wendell, K.D., Emery, J.P., 2010. Inverted fluvial features in the Aeolis/Zephyria Plana region, Mars: Formation mechanism and initial paleodischarge estimates. *J. Geophys. Res.* 115, E07011. <http://dx.doi.org/10.1029/2009JE003496>.
- Carlston, C.W., 1965. The relation of free meander geometry to stream discharge and its geomorphic implications. *Am. J. Sci.* 263, 864–885.
- Carr, M.H., 1983. Stability of streams and lakes on Mars. *Icarus* 56, 476–495.
- Carr, M.H., 1996. *Water on Mars*. Oxford University Press, New York, 229pp.
- Carr, M.H., Evans, N., 1980. *Images of Mars: The Viking Extended Mission*. U.S. Govt. Printing Office, Washington, DC, 32pp.
- Carter, L.M. et al., 2009. Shallow radar (SHARAD) sounding observations of the Medusae Fossae Formation, Mars. *Icarus* 199, 295–302. <http://dx.doi.org/10.1016/j.icarus.2008.10.007>.
- Chander, G., Markham, B., Helder, D., 2009. Summary of current radiometric calibration coefficients for Landsat MSS, TM, ETM+, and EO-1 ALI sensors. *Rem. Sens. Environ.* 113, 893–903.
- Christensen, P.R. et al., 2004. The Thermal Emission Imaging System (THEMIS) for the Mars 2001 Odyssey Mission. *Space Sci. Rev.* 110, 85–310.
- Cooper Pedy Regional Times, February 6, 2011. <<http://cooperpedyregionaltimes.wordpress.com/2011/02/06/tour-de-yasi-leaves-far-north-sa-cold-and-flooded/#more-6984>> (accessed 04.03.13).
- Cuffey, K.M., Paterson, W.S.B., 2010. *The Physics of Glaciers*, fourth ed. Academic Press, Burlington, 704pp.
- Dury, G.H., 1976. Discharge prediction, present and former, from channel dimensions. *J. Hydrol.* 30, 219–245.
- Dury, G.H., 1985. Attainable standards of accuracy in the retrodiction of paleodischarge from channel dimensions. *Earth Surface Process. Landforms* 10, 205–213.
- Edgett, K.S., 2005. The sedimentary rocks of Sinus Meridiani: Five key observations from data acquired by the Mars Global Surveyor and Mars Odyssey orbiters. *Mars* 1, 5–58. <http://dx.doi.org/10.1555/mars.2005.0002>.
- Fryirs, K.A., Briery, G.J., 2013. *Geomorphologic Analysis of River Systems*. John Wiley & Sons, West Sussex, UK, 345pp.
- Ghatan, G.J., Head, J.W., 2004. Regional drainage of meltwater beneath a Hesperian-aged south circumpolar ice sheet on Mars. *J. Geophys. Res.* 109, E07006. <http://dx.doi.org/10.1029/2003JE002196>.
- Greeley, R., Kuzmin, R.O., Haberle, R.M., 2001. Aeolian processes and their effects on understanding the chronology of Mars. *Space Sci. Rev.* 96 (1/4), 393–404.
- Harris, D.R., 1980. Exhumed paleochannels in the Lower Cretaceous Cedar Mountain Formation near Green River. *Brigham Young Univ. Geol. Stud.* 27, 51–66.
- Head III, J.W., 2000a. Tests for ancient polar deposits on Mars: Origin of esker-like sinuous ridges (Dorsa Argentea) using MOLA data. *Lunar Planet. Sci.* XXXI, 1116 (abstract).
- Head III, J.W., 2000b. Tests for ancient polar deposits on Mars: Morphology and topographic relationships of esker-like sinuous ridges (Dorsa Argentea) using MOLA data. *Lunar Planet. Sci.* XXXI, 1117 (abstract).
- Head, J.W., Pratt, S., 2001. Extensive Hesperian-aged south polar ice sheet on Mars: Evidence for massive melting and retreat, and lateral flow and ponding of meltwater. *J. Geophys. Res.* 106, 12275–12299. <http://dx.doi.org/10.1029/2000JE001359>.
- Hiesinger, H., Head, J.W., 2002. Topography and morphology of the Argyle basin, Mars: Implications for its geologic and hydrologic history. *Planet. Space Sci.* 50, 939–981. [http://dx.doi.org/10.1016/S0032-0633\(02\)00054-5](http://dx.doi.org/10.1016/S0032-0633(02)00054-5).
- Hou, B., Frakes, L.A., Sandiford, M., Worrall, L., Keeling, J., 2008. Cenozoic Eucua Basin and associated palaeovalleys, southern Australia – Climatic and tectonic influences on landscape evolution, sedimentation and heavy mineral accumulation. *Sediment. Geol.* 203, 112–130.
- Howard, A.D., 1981. Etched Plains and Braided Ridges of the South Polar Region of Mars: Features Produced by Basal Melting of Ground Ice? NASA Technical Memorandum 84211, Washington, DC, pp. 286–288.
- Irwin III, R.P., Craddock, R.A., Howard, A.D., 2005. Interior channels in martian valley networks: Discharge and runoff production. *Geology* 336, 489–492. <http://dx.doi.org/10.1130/G21333.1>.
- Irwin III, R.P., Howard, A.D., Craddock, R.A., 2008. Fluvial valley networks on Mars. In: Rice, S., Roy, A., Rhoads, B. (Eds.), *River Confluences, Tributaries, and the Fluvial Network*. John Wiley and Sons, West Sussex, UK, pp. 409–430, doi:10.1002/9780470760383.ch19.
- Jacobsen, R.E., Burr, D.M., 2012. Paleo-fluvial features in the Western Medusae Fossae Formation, Aeolis and Zephyria Plana, Mars: Elevations and implications. *Lunar Planet. Sci.* XLIII, 2398 (abstract).
- Kargel, J.S., 1993. Geomorphic processes in the Argyle–Dorsa Argentea region of Mars. *Lunar Planet. Sci.* XXIV, 753–754 (abstract).
- Kargel, J.S., 2004. *Mars: A Warmer Wetter Planet*. Springer, Chichester, UK, 550pp.
- Kargel, J.S., Strom, R.G., 1991. Terrestrial glacial eskers: Analogs for martian sinuous ridges. *Lunar Planet. Sci.* XXII, 683–684 (abstract).

- Kargel, J.S., Strom, G., 1992. Ancient glaciation on Mars. *Geology* 20, 3–7. doi:10.1130/0091-7613(1992)020<0003:AGOM>2.3.CO;2.
- Kerber, L., Head III, J.W., 2010. The age of the Medusae Fossae Formation: Evidence of Hesperian Emplacement from Crater Morphology, Stratigraphy, and Ancient Lava Contacts. *Icarus* 206, 669–684. <http://dx.doi.org/10.1016/j.icarus.2009.10.001>.
- Knighton, D., 1998. Fluvial Forms and Processes. John Wiley & Sons Inc., pp. 352.
- Komar, P.D., 1980. Modes of sediment transport in channelized water flows with ramifications to the erosion of the martian outflow channels. *Icarus* 42, 317–329. [http://dx.doi.org/10.1016/0019-1035\(80\)90097-4](http://dx.doi.org/10.1016/0019-1035(80)90097-4).
- Lang, N.P., 2007. Sinuous ridge formation in southeastern Argyre Planitia, Mars. *Lunar Planet. Sci.* XXXVIII, 1116 (abstract).
- LeDeit, L., Bourgeois, O., Mège, D., Hauber, E., Le Mouélic, S., Massé, M., Jaumann, R., Bibring, J.-P., 2010. Morphology, stratigraphy, and mineralogical composition of a layered formation covering the plateaus around Valles Marineris, Mars: Implications for its geological history. *Icarus* 208, 684–703.
- Lefort, A., Burr, D.M., Beyer, R.A., Howard, A.D., 2012. Inverted fluvial features in the Aeolis–Zephyria Plana, western Medusae Fossae Formation, Mars: Evidence for post-formation modification. *J. Geophys. Res.* 117, 24. <http://dx.doi.org/10.1029/2011JE004008>.
- Maizels, J.K., 1987. In: Frostick, L., Reid, L. (Eds.), Plio-Pleistocene Raised Channel Systems of the Western Sharqiya (Wahiba), Oman. Ancient and Modern, Desert Sediments, pp. 31–50.
- Malin, M.C., Edgett, K.S., 2000a. Sedimentary rocks on Mars. *Science* 290, 1927–1937.
- Malin, M.C., Edgett, K.S., 2000b. Evidence for recent groundwater seepage and surface runoff on Mars. *Science* 288, 2330–2335.
- Malin, M.C., Edgett, K.S., 2003. Evidence for persistent flow and aqueous sedimentation on early Mars. *Science* 302, 1931–1934.
- Malin, M.C. et al., 2007. Context camera investigation on board the Mars Reconnaissance Orbiter. *J. Geophys. Res.* 112. <http://dx.doi.org/10.1029/2006JE002808>.
- Malin, M.C. et al., 2010. An overview of the 1985–2006 Mars Orbiter Camera science investigation. *Mars* 5, 1–60.
- Mandt, K.E., de Silva, S.L., Zimbelman, J.R., Crown, D.A., 2008. The origin of the Medusae Fossae Formation, Mars: Insights from a synoptic approach. *J. Geophys. Res.* 113, E12011. <http://dx.doi.org/10.1029/2008JE003076>.
- Mars Channel Working Group, 1983. Channels and Valleys on Mars. *Geol. Soc. Am. Bull.* 94, 1035–1054.
- McEwen, A.S., Preblich, B.S., Turtle, E.P., Artemieva, N.A., Golombek, M.P., Hurst, M., Kirk, R.L., Burr, D.M., Christensen, P.R., 2005. The rayed crater Zunil and interpretations of small impact craters on Mars. *Icarus* 176 (2), 351–381.
- McEwen, A.S. et al., 2007. Mars Reconnaissance Orbiter's High Resolution Imaging Science Experiment (HiRISE). *J. Geophys. Res.* 112. <http://dx.doi.org/10.1029/2005JE002605>.
- McNally, H.H., Wilson, I.R., 1995. The Mirackina Conglomerate. *Quaternary Geology Notes*, Geological Survey of South Australia, 49, 2–6.
- McNally, G.H., Wilson, I.R., 1996. Silcretes of the Mirackina Palaeochannel, Arckaringa, South Australia. *J. Aust. Geol. Geophys.* 16, 295–301.
- Moore, J.M., Howard, A.D., 2005. Large alluvial fans on Mars. *J. Geophys. Res.* 110, E04005. <http://dx.doi.org/10.1029/2004JE002352>.
- Moore, J.M., Howard, A.D., Dietrich, W.E., Schnek, P.M., 2003. Martian layered fluvial deposits: Implications for Noachian climate scenarios. *Geophys. Res. Lett.* 30, 2292. <http://dx.doi.org/10.1029/2003GL019002>.
- Osterkamp, W.R., Hedman, E.R., 1982. Perennial-Streamflow Characteristics Related to Channel Geometry and Sediment in Missouri River Basin. United States Geological Survey Professional Paper, 1242, 37pp.
- Pain, C.F., Clarke, J.D.A., 2009. Relief inversion: Australian analogs of a common feature of martian landscape evolution. *Lunar Planet. Sci.* XL, 1100 (abstract).
- Pain, C.F., Clarke, J.D.A., Thomas, M., 2007. Inversion of relief on Mars. *Icarus* 190, 478–491.
- Ruff, S.W., Greeley, R., 1990. Sinuous ridges of the south polar region, Mars: Possible origins. *Lunar Planet. Sci.* XXI, 1047–1048 (abstract).
- Schumm, S.A., 2005. River Variability and Complexity. Cambridge University Press, Cambridge, 220pp.
- Scott, D.H., Tanaka, K.L., 1982. Ignimbrites of Amazonis Planitia region of Mars. *J. Geophys. Res.* 87 (B2), 1179–1190.
- Scott, D.H., Tanaka, K.L., 1986. Geological Map of the Western Equatorial Region of Mars. United States Geological Survey Miscellaneous Investigations Series, Map I-1802-A.
- Shean, D.E., Fahle, J., Malin, M.C., Edwards, L.J., Posiolova, L., 2011. MRO CTX stereo image processing and preliminary DEM quality assessment. *Lunar Planet. Sci.* LXII, 2646 (abstract).
- Shreve, R.L., 1985. Esker characteristics in terms of glacier physics, Katahdin esker system, Maine. *Geol. Soc. Am. Bull.* 96, 639–646.
- Tanaka, K.L., 1986. The stratigraphy of Mars. *J. Geophys. Res.* 91, E139–E158.
- Tanaka, K.L., Scott, D.H., 1987. Geologic Map of the Polar Regions of Mars. U.S. Geol. Surv. Misc. Invest. Map, I-1802-C.
- Taylor, J.R., 1982. An Introduction to Error Analysis: The Study of Uncertainties in Physical Measurements. Univ. Sci. Books, Sausalito, Calif, 327pp.
- Watters, T. et al., 2007. Radar sounding of the Medusae Fossae Formation Mars: Equatorial ice or dry, low-density deposits? *Science*. <http://dx.doi.org/10.1126/science.1148112>.
- Weitz, C.M., Milliken, R.E., Grant, J.A., McEwen, A.S., Williams, R.M.E., Bishop, J.L., Thomson, B.J., 2010. Mars Reconnaissance Orbiter observations of light-toned layered deposits and associated fluvial landforms on the plateaus adjacent to Valles Marineris. *Icarus* 205, 73–102.
- West, M.D., Clarke, J.D.A., Thomas, M., Pain, C.F., Walter, M.R., 2010. The geology of Australian Mars analogue sites. *Planet. Space Sci.* 58, 447–458.
- Williams, G.P., 1984. Palaeohydrological equations for rivers. In: Costa, J.E., Fleisher, P.J. (Eds.), *Developments and Applications of Geomorphology*. Springer-Verlag, New York, pp. 343–367.
- Williams, G.P., 1988. Paleofluvial estimates from dimensions of former channels and meanders. In: Baker, V.R., Kochel, R.C., Patton, P.C. (Eds.), *Flood Geomorphology*. John Wiley and Sons, New York, pp. 321–334.
- Williams, R.M.E., 2007. Global Spatial Distribution of Raised Curvilinear Features on Mars. *Lunar Planet. Sci.* XXXVIII, 1821 (abstract).
- Williams, R.M.E., Chuang, F.C., 2012. Mapping of Sinuous Ridges in Oxia Palus, Mars: New Insight into the Aqueous Record. *Lunar Planet. Sci.* XLIII, Abstract #2156.
- Williams, R.M.E., Edgett, K.S., 2005. Valleys in the martian rock record. *Lunar Planet. Sci.* XXXVI, 2099 (abstract).
- Williams, R.M.E., Irwin III, R.P., Zimbelman, J.R., 2009. Evaluation of paleohydrologic models for terrestrial inverted channels: Implications for application to martian sinuous ridges. *Geomorphology* 107, 300–315.
- Wilson, L., Ghatan, G.J., Head III, J.W., Mitchell, K.L., 2004. Mars outflow channels: A reappraisal of the estimation of water flow velocities from water depths, regional slopes, and channel floor properties. *J. Geophys. Res.* 109, E09003. <http://dx.doi.org/10.1029/2004JE002281>.
- Zimbelman, J.R., 2011. Preliminary Geologic Map of the MC-23 NW Quadrangle, Mars: Lower Member of the Medusae Fossae Formation. *Lunar Planet. Sci.* XXXII, 1840 (abstract).
- Zimbelman, J.R., Griffin, L.J., 2010. HiRISE images of yardangs and sinuous ridges in the lower member of the Medusae Fossae Formation, Mars. *Icarus*, 198–210.
- Zimbelman, J.R., Scheidt, S.P., 2012. Hesperian age for western Medusae Fossae Formation, Mars. *Science* 336, 1683. <http://dx.doi.org/10.1126/science.1221094>.
- Zimbelman, J.R., Crown, D.A., Grant, J.A., Hooper, D.M., 1997. The Medusae Fossae Formation, Amazonis Planitia, Mars: Evolution of proposed hypotheses of origin. *Lunar Planet. Sci.* XXVIII, Abstract 1482.